A national laboratory of the U.S. Department of Energy
Office of Energy Efficiency & Renewable Energy

National Renewable Energy Laboratory

Innovation for Our Energy Future

Loads Analysis of a Floating Offshore Wind Turbine Using Fully Coupled Simulation

Preprint

J.M. Jonkman and M.L. Buhl, Jr.

To be presented at WindPower 2007 Conference & Exhibition
Los Angeles, California
June 3–6, 2007

Conference Paper
NREL/CP-500-41714
June 2007

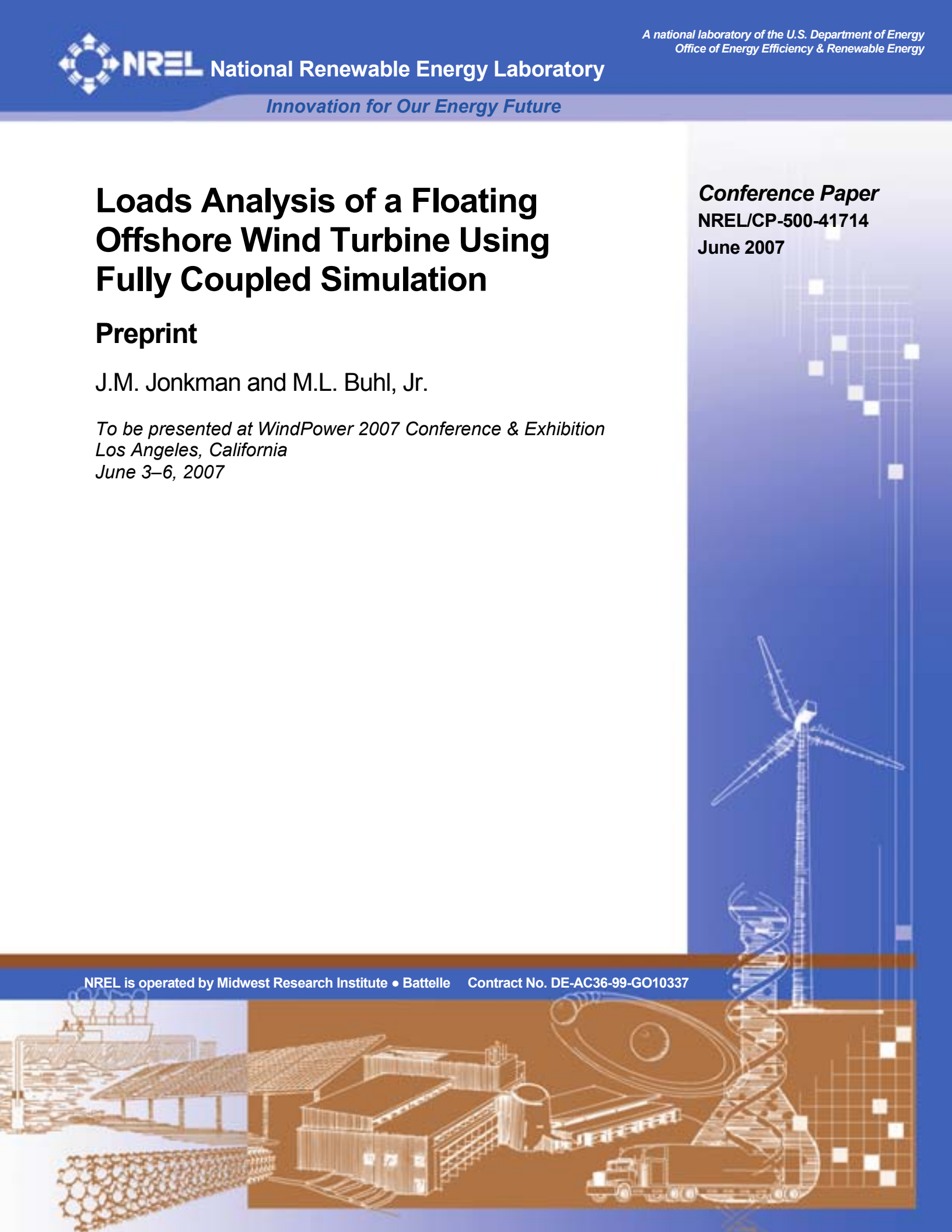

NREL is operated by Midwest Research Institute • Battelle Contract No. DE-AC36-99-GO10337

Loads Analysis of a Floating Offshore Wind Turbine Using Fully Coupled Simulation*

Jason M. Jonkman and Marshall L. Buhl Jr.
National Renewable Energy Laboratory (NREL), Golden, Colorado, 80401-3393

The vast deepwater wind resource represents a potential to use floating offshore wind turbines to power much of the world with renewable energy. Comprehensive simulation tools that account for the coupled excitation and response of the complete system, including the influences of wind-inflow, aerodynamics, structural dynamics, controls, and, for offshore systems, waves, currents, and hydrodynamics, are used to design and analyze wind turbines. The application of such tools in the analysis of floating offshore wind turbines has previously been investigated to only a limited extent. There are numerous possible concepts for floating offshore wind turbine platforms, including a variety of configurations currently used in the offshore oil and gas industries. Coupled analyses are needed to determine their technical and economic feasibility. This paper presents the use of fully coupled aero-hydro-servo-elastic simulation tools to perform a preliminary loads analysis of a 5-MW offshore wind turbine supported by a barge with catenary moorings, which is one of the many promising floating platform concepts. A barge platform was chosen because of its simplicity in design, fabrication, and installation. The aim of the loads analysis was to characterize the dynamic response and to identify potential loads and instabilities that would be detrimental to the concept. A comparison was made between the response of the floating system and the response of the turbine installed on land to quantify the impact brought about by the dynamic couplings between the turbine and floating barge in the presence of combined wind and wave loading. The coupling between the wind turbine response and the barge pitch motion, in particular, was found to produce larger extreme loads in the floating turbine, especially in its tower, but also in its blades. The barge was found to be susceptible to excessive pitching in extreme wave conditions. Relative to the fixed land-based support, the added compliance in the barge led to an instability of the floating system in yaw when the wind turbine was idling with a faulted blade. The compliance of the floating barge did however mitigate a tower side-to-side instability discovered in the land-based turbine. Design modifications for reducing the barge motions, improving the turbine response, and eliminating the instabilities are suggested to obtain a cost effective design that achieves favorable performance while maintaining structural integrity.

Nomenclature

$E[H_s,V_{hub}]$	=	expected value of the significant wave height conditioned on the mean hub-height wind speed, based on the long-term joint probability distribution of metocean parameters
H_s	=	significant wave height
H_{s50}	=	significant wave height, based on a 3-h reference period, with a recurrence period of 50 yr
H_{s1}	=	significant wave height, based on a 3-h reference period, with a recurrence period of 1 yr
T_p	=	peak spectral period
V_{50}	=	reference 10-min average wind speed with a recurrence period of 50 yr
V_1	=	reference 10-min average wind speed with a recurrence period of 1 yr
V_{hub}	=	hub-height wind speed averaged over a given reference period

V_{out} = cut-out wind speed
V_r = rated wind speed
β = incident wave propagation heading direction

I. Introduction

IN Europe, where vacant land is scarce and vast shallow water wind resources are available, more than 900 MW of offshore wind energy capacity has been installed in and around the North and Baltic Seas.[1] Although offshore wind turbines are not currently installed outside Europe, interest is growing worldwide because the global offshore wind resource is abundant, with the U.S. potential ranked second only to China.[2] For instance, the wind resource potential at 5 to 50 nautical miles off the U.S. coast is estimated to be more than the total currently installed electrical generating capacity of the United States (more than 900 GW).[3]

Most of the offshore wind resource potential in the United States, China, Japan, Norway, and many other countries is available in water deeper than 30 m. In contrast, all of the European offshore wind turbines installed to date are fixed-bottom substructures, and have mostly been installed in water shallower than 20 m by driving monopiles into the seabed or by relying on conventional concrete gravity bases. These technologies are not economically feasible in deeper water. Instead, space frame substructures, including tripods, quadpods, or lattice frames (e.g., "jackets"), will be required to maintain the strength and stiffness requirements at the lowest possible cost. The Beatrice Wind Farm Demonstrator Project, where two 5-MW wind turbines will be installed on a jacket structure in 45 m of water, is a good example of this technology.[†] At some depth, however, floating support platforms will be the most economical. This natural progression is illustrated in Fig. 1.[4] Without performing a dynamic analysis, Musial, Butterfield, and Boone have demonstrated the economic potential of one floating platform design.[2]

Numerous floating support platform configurations are possible for offshore wind turbines when one considers

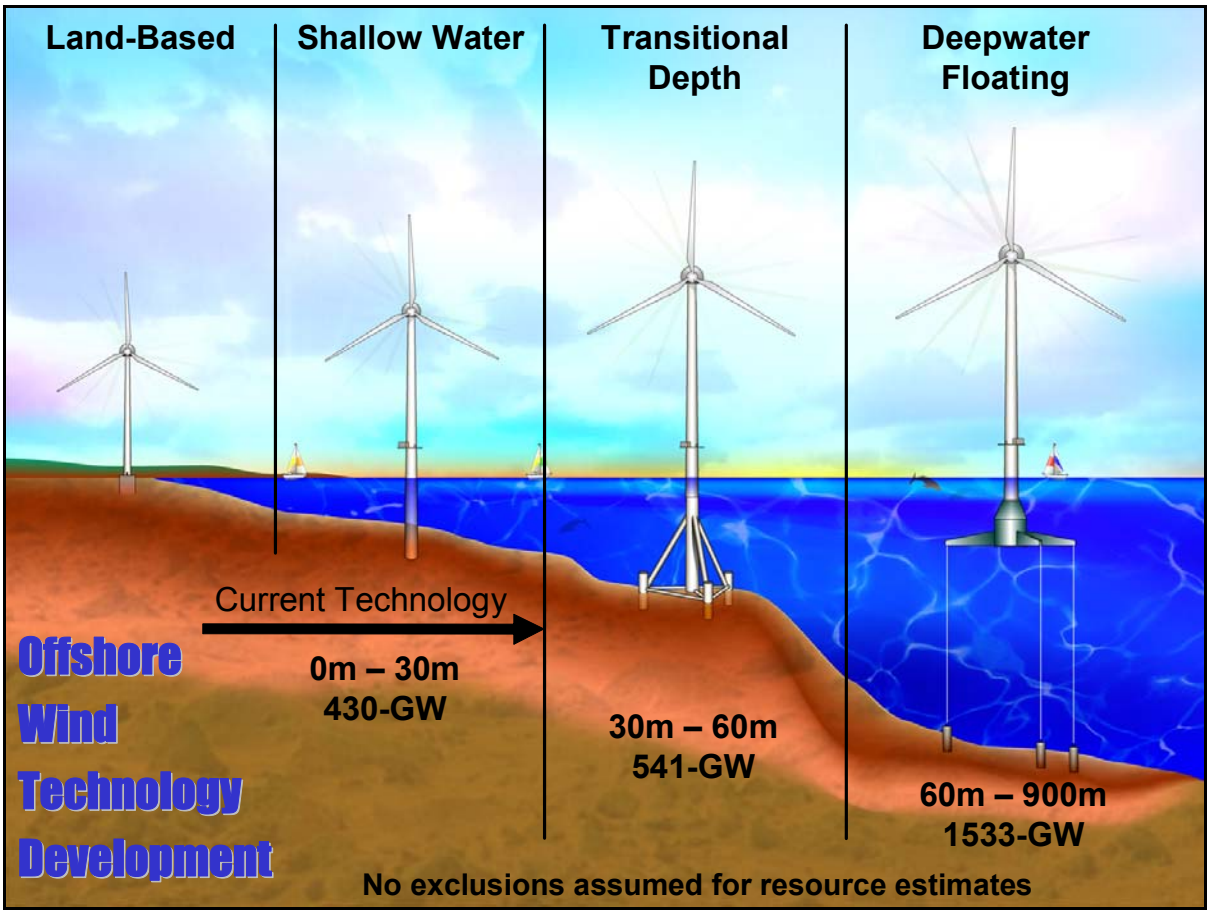

Figure 1. The natural progression of substructure designs from shallow to deep water.

[†] Website: http://www.beatricewind.co.uk/home/default.asp.

the variety of mooring systems, tanks, and ballast options that are used in the offshore oil and gas industries. Figure 2 illustrates several of the concepts, which are classified in terms of how the designs achieve static stability. The Spar-buoy concept achieves stability by using ballast to lower the center of gravity below the center of buoyancy and can be moored by catenary or taut lines. The Tension Leg Platform (TLP) achieves stability through the use of mooring line tension brought about by excess buoyancy in the tank. The barge concept achieves stability through its waterplane area and is generally moored by catenary lines. Hybrid concepts, which use features from all three classes, are also an option.[5]

Recently, a variety of studies have assessed the preliminary design of floating offshore wind turbines. Many of these studies used linear frequency-domain analysis, which is commonly employed in the offshore oil and gas industry. For example, Bulder et al[6] used linear frequency-domain hydrodynamics techniques to find the Response Amplitude Operators (RAOs) and amplitude standard deviations of the six rigid-body modes of motion for the support platform of a tri-floater design for a 5-MW wind turbine. A similar process was used by Lee[7] to analyze a TLP design and a taut-leg Spar-buoy design for 1.5-MW wind turbine, and by Wayman, Sclavounos, Butterfield, Jonkman, and Musial[8,9] to analyze multiple TLP designs and a shallow drafted barge design for a 5-MW wind turbine. Most recently, through frequency domain analysis, Vijfhuizen designed a barge for a 5-MW wind turbine, which is also a platform for an oscillating water column (OWC) wave-energy device.[10] In these studies, the attributes of the wind turbine were included by augmenting the body mass matrix with the mass properties of the turbine and by augmenting the hydrodynamic damping and restoring matrices with damping and restoring contributions from rotor aerodynamics and gyroscopics. Additionally, the linearized restoring properties of the mooring system were derived about a mean offset displacement of the support platform caused by the aerodynamic thrust on the rotor. The elasticity of the wind turbine was ignored. All of the studies demonstrated the technical feasibility of floating offshore wind turbines by showing that, through proper design, the natural frequencies of the floating support platform could be placed where there is little energy in the wave spectrum to ensure that the dynamic response is minimized.

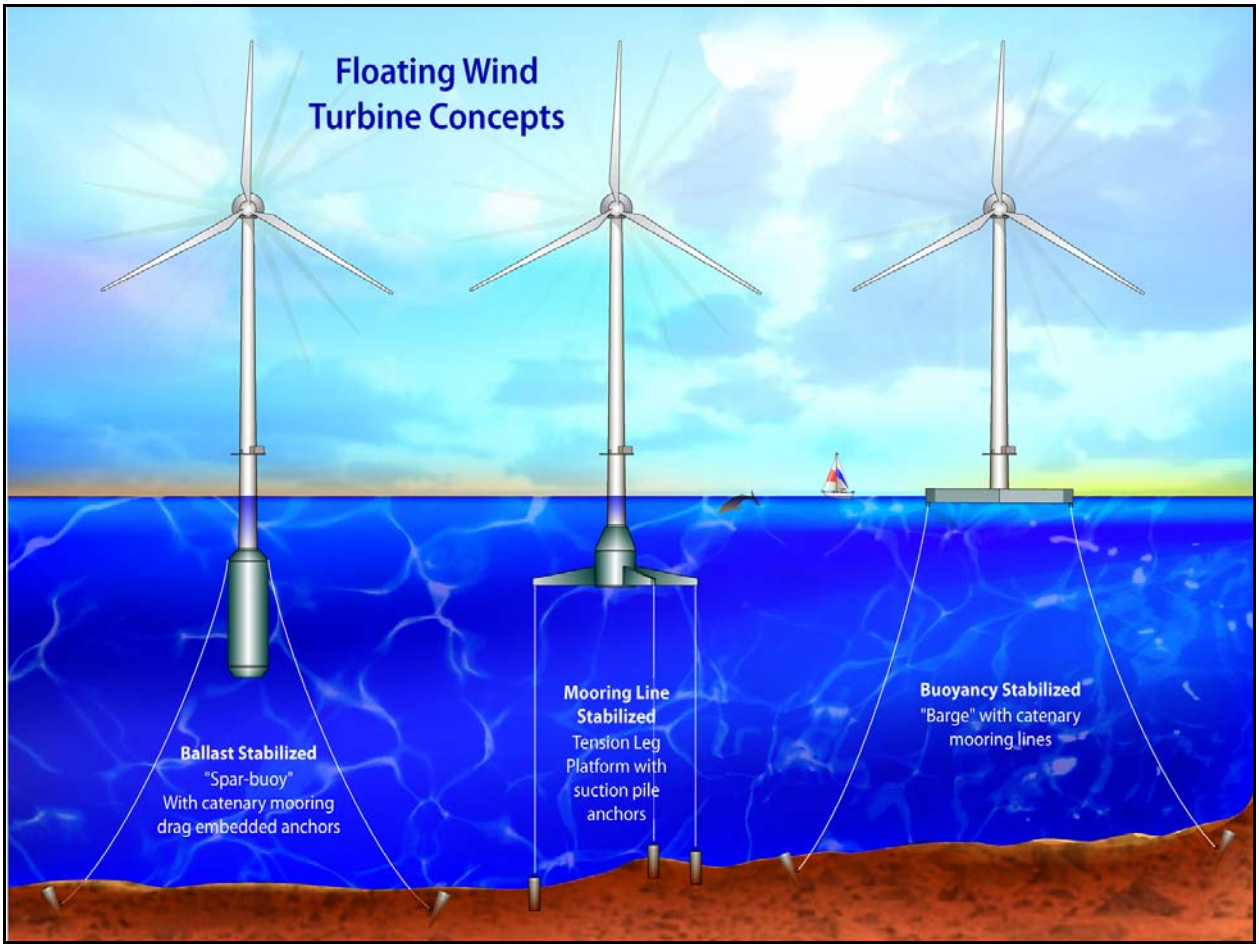

Figure 2. Floating support platform concepts for offshore wind turbines.

One limitation of these linear frequency-domain analyses is that they cannot capture nonlinear dynamic characteristics and transient events that are important considerations in the analysis of wind turbines. Several offshore floating wind turbine studies have addressed this limitation. Using a state-domain technique, Henderson and Patel[11] used RAOs to prescribe the motions of a 700-kW wind turbine to determine the effect platform motions have on turbine fatigue loads. They showed that platform motions have little effect on power capture and rotor loads; instead, these are dominated by the aerodynamics of the rotor. However, they also showed that platform motions have a substantial effect on the nacelle and tower loads, which are dominated by inertia; thus, the tower will have to be strengthened if the platform motions cannot be reduced. The same conclusions were drawn independently by Fulton, Malcolm, and Moroz,[12] and Withee,[13] who used different time-domain aeroelastic wind turbine simulators that had been adapted to include the effects of platform motion and hydrodynamic loading of TLP designs for a 5-MW and 1.5-MW wind turbine, respectively. Likewise, similar conclusions were drawn from a more recent analysis by Neilsen, Hanson, and Skaare,[14,15] who used a coupled aeroelastic, hydrodynamic, and mooring program to design a deep-drafted Spar-buoy (called "Hywind") to support a 5-MW wind turbine and to develop its corresponding control system. This study, in particular, was important because the computer program simulations were verified by the response of a scaled-down model in a wave tank experiment. Finally, Zambrano, MacCready, Kiceniuk, Roddier, and Cermelli[16,17] demonstrated the technical (but not economic) feasibility of smaller floating wind turbines by using a time domain model to determine the support platform motions and mooring tensions for a semi-submersible platform supporting three wind turbines of either 90 kW or 225 kW each and a TLP supporting a single 1-kW turbine.

Limitations in these studies must also be addressed. For instance, the time domain dynamics models employed by Fulton, Malcolm, and Moroz, and Withee used Morison's equation[18,19] to compute the hydrodynamic loading on the TLPs. Morison's equation ignores many effects that are important to analysis of more general support platform configurations, such as the effects of platform size in the diffraction problem, wave radiation damping and free-surface memory, and added mass-induced coupling between modes of motion.[20,21] Although the hydrodynamics model was more sophisticated in the time domain dynamics program employed by Zambrano, MacCready, Kiceniuk, Roddier, and Cermelli, their aerodynamics and structural dynamics models were unsophisticated, consisting only of a single horizontal drag force for the aerodynamics model and the six rigid-body modes of motion of the support platform for the structural dynamics model. Also, the concept analyzed by Neilsen, Hanson, and Skaare has such a large draft (120 m), that it would be difficult to construct and only be deployable at very deep sites. Moreover, the findings and conclusions drawn by all of the previous studies must be verified through a rigorous loads analysis.

The International Electrotechnical Commission (IEC) 61400–1 design standard[22] specifies the design requirements for land-based wind turbines and the IEC 61400–3 design standard[23] supplements the 61400–1 design standard with design requirements for sea-based wind turbines. Both design standards require that an integrated loads analysis be performed when a machine is certified. Such analysis is also beneficial for design and analysis, to obtain cost-effective wind turbines that achieve favorable performance, and maintain structural integrity. Integrated loads analyses are carried out with comprehensive time-domain simulation tools that employ sophisticated models of both turbulent and deterministic wind-inflow; aerodynamic, gravitational, and inertial loading of the rotor, nacelle, and tower; elastic effects within and between components and in the foundation; and mechanical actuation and electrical responses of the generator and control and protection systems. For offshore wind turbines, additional models of the hydrodynamic loading in regular and irregular seas, the dynamic coupling between the support platform motion and wind turbine motion, and the dynamic characterization of mooring systems for compliant floating platforms are also necessary.

This paper is a continuation of the work presented previously by Jonkman and Sclavounos[24] and Jonkman and Buhl,[25] which introduced the development and verification of a comprehensive simulation tool that can model the fully coupled aero-hydro-servo-elastic response of offshore floating wind turbines. Our offshore floating wind turbine simulator was developed with enough sophistication to address the limitations of the previous time and frequency domain studies and to have the features required to perform an integrated loads analysis for a variety of wind turbine, support platform, and mooring system configurations. A summary of the simulation capabilities is given in section II. We then present a preliminary loads analysis, carried out by application of the simulation tool and guided by the IEC design standards, for a 5-MW wind turbine supported both on land and offshore by a floating barge with slack, catenary moorings. The loads analysis not only allowed us to characterize the dynamic response of the land- and sea-based systems, but by comparing both responses, we can quantify the impact brought about by dynamic coupling between the turbine and floating barge in the presence of combined wind and wave loading. The results of comprehensive loads analyses for some of the other promising offshore floating wind turbine configurations will be presented in future papers.

II. Fully Coupled Aero-Hydro-Servo-Elastic Simulation

Limitations of previous time and frequency domain studies on floating offshore wind turbines motivated our development of simulation capability for modeling the fully coupled aero-hydro-servo-elastic response of such systems. This capability has been developed by combining the computational methodologies of the onshore wind turbine and offshore oil and gas industries. The onshore wind industry-accepted aero-servo-elastic turbine simulation capabilities of FAST[26] with AeroDyn[27,28] and MSC.ADAMS®‡ with A2AD[29,30] and AeroDyn have been interfaced with the external hydrodynamic wave-body interaction program WAMIT®,[31] which is commonly employed in the offshore oil and gas industry. These interfaces have been supported by the development of modules for treating time domain hydrodynamics (HydroDyn) and quasi-static mooring system responses. A rundown of the modules and their interfaces is given in Fig. 3. Please note that we use the term "ADAMS" to imply "MSC.ADAMS® with A2AD" in this paper.

Turbulent wind-inflow is prescribed by an external computer program TurbSim[32] and (not shown in Fig. 3) deterministic wind-inflow is prescribed by an external computer program IECWind.[33] FAST with AeroDyn and ADAMS with AeroDyn account for the applied aerodynamic and gravitational loads, the behavior of the control and protection systems, and the structural dynamics of the wind turbine. The latter contribution includes the elasticity of the rotor, drivetrain, and tower, and the dynamic coupling between the motions of the support platform and the motions of the wind turbine. (FAST and ADAMS are separate programs that may be run independently to model the structural dynamic response and control system behavior of wind turbines. FAST employs a combined modal and multibody structural dynamics formulation, whereas ADAMS employs a higher-fidelity multibody formulation. They have both been interfaced with AeroDyn to enable the full aero-servo-elastic modeling of wind turbines). Nonlinear restoring loads from the mooring system are obtained from a quasi-static mooring line module that accounts for the elastic stretching of an array of homogenous taut or slack catenary lines with seabed interaction. HydroDyn is a module that computes the applied hydrodynamic loads in the time domain. Accounted for in the model are linear hydrostatic restoring; nonlinear viscous drag from incident wave kinematics, sea currents, and platform motion; the added mass and damping contributions from linear wave radiation, including free surface memory effects; and the incident wave excitation from linear diffraction in regular or irregular seas. Just as aerodynamic loads depend on the shape of the rotor blade airfoils, so do hydrodynamic loads depend on the support platform's geometry. To this end, HydroDyn was developed such that the hydrodynamic coefficients for platforms of arbitrary shape are imported from WAMIT or an equivalent hydrodynamic preprocessor. (WAMIT uses a three-dimensional, numerical panel method to solve the linearized radiation and diffraction problems for the interaction of surface waves with offshore platforms in the frequency-domain.) References 24 and 25 explain the theoretical framework and limitations of the hydrodynamic and mooring system modules in detail. In addition, Ref. 25 presents a model-to-model verification of these modules and of the fully coupled simulation tool.

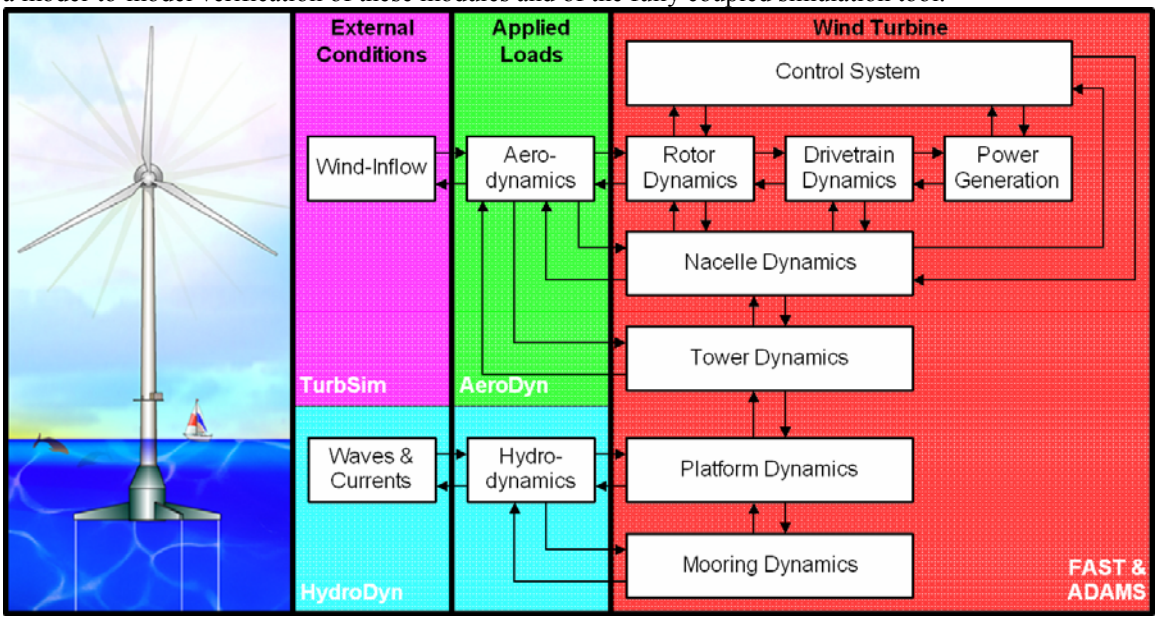

Figure 3. Interfacing modules to achieve fully coupled aero-hydro-servo-elastic simulation.

‡ Website: http://www.mscsoftware.com.

By interfacing these modules as described, fully coupled, time domain, aero-hydro-servo-elastic simulation of offshore floating wind turbines is achieved. This is crucial for analyzing the dynamic response from combined wind and wave loading because both can affect the motions, loads, and power production of the system. The generality of each module also ensures that the overall simulation tool is universal enough to analyze a variety of wind turbine, support platform, and mooring system configurations. Moreover, the same simulation tool can still be used to model land-based wind turbines by disabling the hydrodynamic and mooring system modules.

III. Design Basis and Wind Turbine Model

To obtain useful information from this and other concept studies aimed at assessing offshore wind technology that is suitable in the deep waters off the U.S. Offshore Continental Shelf and other offshore sites worldwide, use of realistic and standardized input data is required. This section summarizes the input data we used in our preliminary loads analysis. A large collection of input data is needed, including detailed specifications of the wind turbine and support platform, and a design basis. A design basis consists of the analysis methods (see section II), a collection of the applicable design standards (i.e., IEC), and the site-specific meteorological and oceanographic (metocean) parameters at a reference site. In this study, we used wind turbine specifications of the National Renewable Energy Laboratory's (NREL's) offshore 5-MW baseline turbine, and support platform specifications of a barge from ITI Energy. We selected a location in the northern North Sea as the reference site.

A. NREL Offshore 5-MW Baseline Wind Turbine

The NREL offshore 5-MW baseline wind turbine has been used to establish the reference specifications for a number of research projects supported by the U.S. Department of Energy's Wind Energy Technologies Program.[8,9,12,25,34,35] In addition, the integrated European Union UpWind research program[§] and the International Energy Agency Wind Annex XXIII Offshore Code Comparison Collaborative[**] have adopted the NREL offshore 5-MW baseline wind turbine as their reference model. The model has been, and will continue to be, used as a reference by research teams throughout the world to standardize baseline offshore wind turbine specifications and to quantify the benefits of advanced land- and sea-based wind energy technologies.

The 5-MW rating is large by today's standards, but is assumed to be the minimum rating necessary to make a floating wind turbine system economical because of the large proportion of the costs in the support platform. The wind turbine design is typical of utility-scale, land- and sea-based, multi-megawatt turbines. To create the model, we obtained some broad design information from the published documents of turbine manufacturers, with a heavy emphasis on the REpower 5M.[††] Because detailed data was unavailable, however, we used typical, preliminary design methods to arrive at the specifications required to build sophisticated models, including definitions of the aerodynamic, structural dynamic, and control system properties. Table 1 summarizes some of these properties. More detail is available in Ref. 36.

Table 1. Summary of baseline wind turbine properties.

Rating	5 MW
Rotor Orientation	Upwind
Control	Variable Speed, Collective Pitch
Drivetrain	High Speed, Multiple Stage Gearbox
Rotor Diameter	126 m
Hub Height	90 m
Cut-In, Rated, Cut-Out Wind Speed	3 m/s, 11.4 m/s, 25 m/s
Cut-In, Rated Rotor Speed	6.9 rpm, 12.1 rpm
Rated Tip Speed	80 m/s
Overhang, Shaft Tilt, Precone	5 m, 5°, 2.5°
Rotor Mass	110,000 kg
Nacelle Mass	240,000 kg
Tower Mass	347,460 kg
Overall Center of Mass	(−0.2 m, 0.0 m, 64.0 m)

[§] Website: http://www.upwind.eu/default.aspx.
[**] Website: http://www.ieawind.org/Annex%20XXIII/Subtask2.html.
[††] Website: http://www.repower5m.com/index_flash_uk.htm.

B. ITI Energy Barge

We mounted the 5-MW wind turbine on a floating barge in our sea-based loads analysis. We used a preliminary barge design, as developed by the Department of Naval Architecture and Marine Engineering at the Universities of Glasgow and Strathclyde through a contract with ITI Energy. A barge concept was chosen by ITI Energy because of its simplicity in design, fabrication, and installation. Not only is the barge designed to support the NREL offshore 5-MW baseline wind turbine, but it is also a platform for an OWC wave power device. To ensure that the simplest possible manufacturing techniques can be used in its fabrication, the barge is square and the wave energy is extracted from a square moonpool located at the center of the barge. This allows the OWC to be installed within the tower of the wind turbine. The barge is ballasted with sea water to achieve a reasonable draft, which is not too shallow so as to be susceptible to incessant wave slamming. To prevent it from drifting, the platform is moored by a system of eight catenary lines, two of which emanate from each corner of the bottom of the barge, such that they would be 45° apart at the corner. We provide some details of the barge and mooring system in Table 2 and illustrate the concept with an image courtesy of ADAMS in Fig. 4. The concept is documented in much greater detail in Ref. 10.

The capabilities of our simulation tool do not permit us to model an OWC wave power device or their associated potential for energy extraction. Instead, we modeled the hydrodynamics of the barge by assuming that the moonpool was covered over by a fixed plate located just below the free surface. Reference 25 explains this assumption in more detail.

Table 2. Summary of ITI Energy barge properties.

Size (W×L×H)	40 m × 40 m × 10 m
Moonpool (W×L×H)	10 m × 10 m × 10 m
Draft, Freeboard	4 m, 6 m
Water Displacement	6,000 m^3
Mass, Including Ballast	5,452,000 kg
Center of Mass (CM) below SWL	0.282 m
Roll Inertia about CM	726,900,000 $kg \cdot m^2$
Pitch Inertia about CM	726,900,000 $kg \cdot m^2$
Yaw Inertia about CM	1,453,900,000 $kg \cdot m^2$
Anchor (Water) Depth	150 m
Separation Between Opposing Anchors	773.8 m
Unstretched Line Length	473.3 m
Neutral Line Length Resting on Seabed	250 m
Line Diameter	0.0809 m
Line Mass Density	130.4 kg/m
Line Extensional Stiffness	589,000,000 N

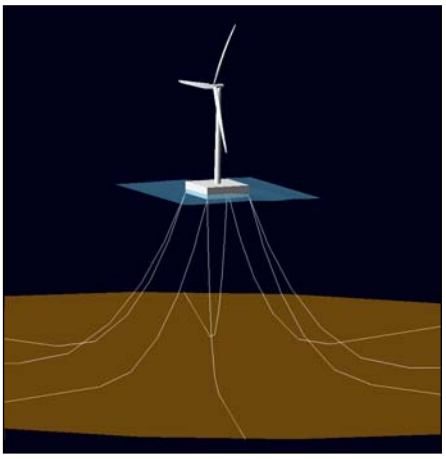

Figure 4. Illustration of the NREL 5-MW wind turbine on the ITI Energy barge.

C. Reference Site Data

The IEC 61400–3 design standard requires that a loads analysis be based on site-specific external conditions.[23] At the request of ITI Energy, we selected the location of the former Stevenson Weather Station as our reference site for which to obtain environmental (metocean) data. This site is located at 61º 20' N latitude, 0º 0' E longitude, on the Prime Meridian northeast of the Shetland Islands northeast of Scotland. Figure 5 illustrates this location with an image courtesy of Google Earth.[‡‡] This reference site was chosen for its fairly extreme wind and wave conditions, with the implication that if the results of the loads analysis are favorable, then the floating wind turbine system under consideration will be applicable at almost any site worldwide.

A Waverider buoy collected short-term wave statistics at this site from February 1973 to February 1976. This dataset did not contain wind speed information however, so it was not directly applicable to our loads analysis, which requires joint wind and wave data. Instead, we purchased wind and wave data at the reference site through the online Waveclimate.com service[§§] that is run by the Advisory and Research Group on Geo Observation Systems and Services (ARGOSS) of The Netherlands.[***] The Waveclimate.com service provides a worldwide database of wind and wave climate information based on a combination of measurements and a global hindcast model. The

[‡‡] Website: http://earth.google.com/.
[§§] Website: http://www.waveclimate.com/.
[***] Website: http://www.argoss.nl/.

measured data come from a composite of radar altimeter, radar scatterometer, and imaging radar [Synthetic Aperture Radar (SAR)] observations, taken from 1985 to present. The Waveclimate.com database has been validated and calibrated with measurements from surface buoys, though not specifically at our chosen reference site. The model is based on the third-generation ocean wind-wave model WaveWatch III, which solves the spectral action density balance equation for wavenumber-direction spectra.[37] Although we don't show any of the comparisons in this paper, the wave data obtained through the Waveclimate.com service agreed quite well with the wave statistics available from the former Waverider buoy. This provided us with confidence in the accuracy of the Waveclimate.com product.

Figure 5. Reference site location.

The Waveclimate.com service uses a grid spacing of 1º latitude by 1º longitude in the vicinity of the reference site. We chose the cell with grid boundaries of 61º to 62º N latitude, 0º to 1º E longitude. We purchased two sets of data for this cell. The first dataset consisted of an estimate of the long-term joint probability distribution of wind speed, significant wave height, and mean wave period. The second dataset was a prediction of the extreme significant wave heights for various return periods.

The joint probability distribution was provided in terms of 37,992 samples, each based on a 3-h reference (averaging) period, representing a total of about 13 years of data. The samples were grouped in bins with a wind speed width of 2 knots (1.029 m/s), a significant wave height width of 1 m, and a mean wave period width of 1 s. The reference elevation for the wind speed data was 10 m above the mean sea level. To adjust this data to the turbine's hub-height of 90 m, we assumed a vertical power-law shear exponent of 0.14 and scaled all of the wind speed bins by a factor of $(90/10)^{0.14} = 1.360$, resulting in an altered bin width of 1.399 m/s for the hub-height wind speed, V_{hub}. We also converted the data of mean wave period to peak spectral period, T_p. By assuming that the wave conditions were represented by the modified Pierson-Moskowitz spectrum, we scaled all of wave period bins by a factor of 1.408,[19] resulting in an altered bin width of 1.408 s. The data of significant wave height, H_s, did not require adjustment.

The resolution of the resulting long-term joint probability distribution does not entirely conform to the maximum bin widths of 2 m/s, 0.5 m, and 0.5 s required by the IEC 61400–3 design standard,[23] but the resolution was deemed adequate because our loads analysis is preliminary in nature. Likewise, we found it acceptable to have the joint probability distribution based on a 3-h reference period instead of the 1-h period required by the –3 design standard. This is because the marginal long-term probability distributions of significant wave height and peak spectral period do not depend on the averaging period, and because the marginal long-term probability distribution of mean wind speed may be assumed to be independent of the averaging period for periods in the range of 10 min to 3 h.[23]

Using the long-term joint probability distribution, we characterized the expected value of the significant wave height, $E[H_s,V_{hub}]$, as well as the range of associated peak spectral periods, conditioned on the mean hub-height wind speed from cut-in to cut-out. The data are presented in Fig. 6. As shown, the expected value of the significant wave height increases with the mean hub-height wind speed that it is conditioned on—from about 1.6 m at cut-in, V_{in} = 3 m/s, to about 5.9 m at cut-out, V_{out} = 25 m/s. The peak spectral periods have a median that increases and a range that tends to decrease with the expected significant wave height they are associated with, from about 12.7±5.6 s at 1.6 m, to about 15.5±4.2 s at 5.9 m.

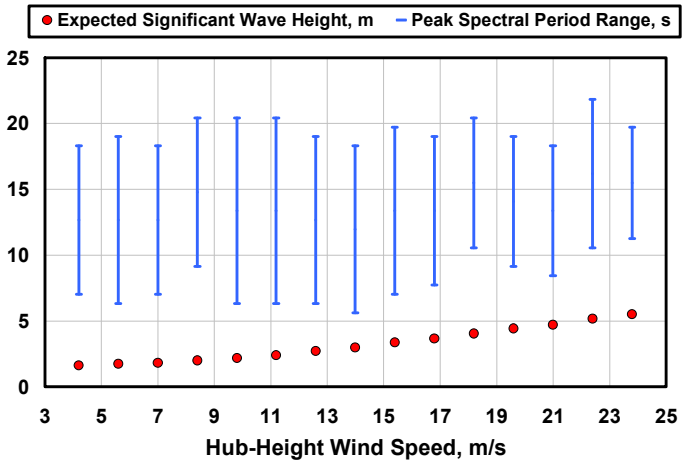

Figure 6. Normal sea state conditions at the reference site.

The extreme value analysis from the Waveclimate.com service provided predictions of the extreme significant wave heights at the reference site for various return periods. The

associated wind and wave period information was not available however, so we had to rely on assumptions and estimates to specify them. Although the –3 design standard[23] requires the estimation of the extreme individual wave heights at the reference site, we did not assess them because we did not use regular, periodic waves in our preliminary loads analysis; instead, we relied on irregular sea states as described in section IV of this paper.

Based on a 3-h reference period, the significant wave height with a recurrence period of 1 yr, H_{s1}, was predicted by the Waveclimate.com service to be 10.8 m, and the significant wave height with a recurrence period of 50 yr, H_{s50}, was predicted to be 13.8 m. We estimated that the range of peak spectral periods associated with the 1-yr recurrence of significant wave height to be 15.5 to 19.7 s from data available in the joint-probability distribution. Because 50-yr recurrence data does not exist in the 13-yr record of joint probability statistics however, we had to extrapolate to estimate the range of peak spectral periods associated with the 50-yr recurrence significant wave height. By this extrapolation, we estimated a range of 18.5 to 19.9 s. We assumed that the extreme wind speeds at the reference site conformed to those prescribed by wind turbine class I from the IEC –1 design standard. Based on this assumption and a 10-min averaging period, the reference hub-height wind speed with a recurrence period of 1 yr, V_1, was prescribed to be 40 m/s and the reference hub-height wind speed with a recurrence period of 50 yr, V_{50}, was prescribed to be 50 m/s.[22]

The water depth at the reference site is roughly 160 m; however, we performed our analysis with a depth of 150 m as indicated in Table 2.

We did not quantify several other commonly assessed environmental conditions at the reference site due again to the preliminary scope of our loads analysis. For some of the unquantified conditions, we assumed typical values. We did not assess, nor did we account for in our loads analysis, the potential loading from, sea ice, marine growth, corrosion, wake effects from neighboring wind turbines in a wind farm, earthquakes, variations in water levels from astronomical tides and storm surges, and sea currents generated by wind, tides, storm surges, atmospheric pressure variations, and near shore waves (i.e., surf currents). We did not assess the soil conditions at the reference site because our simulation tool assumes that the anchor locations of each mooring line are fixed to the inertia frame at the seabed. We assumed standard values of 1.225 kg/m^3 for the air density and 1,025 kg/m^3 for the water density. We assumed a vertical power-law shear exponent of 0.14 for all normal wind conditions, and 0.11 in extreme 1- and 50-yr wind conditions as dictated by the –3 design standard.[23] Likewise, we assumed that the wind turbulence at the reference site conformed to the models prescribed by wind turbine turbulence-category B from the –3 design standard instead of assessing the ambient turbulence standard deviation from site data, or from estimations derived from the surface roughness according to the Charnock expression. The correlation of wind and wave direction was not assessed and we opted instead to use the guidance of the –3 design standard (see section IV). We ignored wave directional spreading and used long-crested waves for all sea states. Finally, we did not prescribe a site-specific wave spectrum and opted instead to use the JOint North Sea WAve Project (JONSWAP) spectrum defined in the –3 design standard. This formulation uses a peak shape parameter derived from the significant wave height and peak spectral period and reduces down to the Pierson-Moskowitz spectrum in all but the most extreme sea states.[23] All of these assumptions and omissions will have to be addressed in more detailed, follow-on loads analysis projects.

IV. Loads Analysis Overview and Description

We ran two preliminary sets of loads analyses. The first loads analysis was for the NREL offshore 5-MW baseline wind turbine installed on land. Its aim was to establish the response of the baseline turbine without the effects of hydrodynamic loading or platform motion. The second loads analysis was for the same wind turbine mounted offshore on the floating ITI Energy barge. The same wind turbine control system was used in both analyses. The use of the same turbine model (identical from blade tip to tower base) and control system in both the on- and offshore load sets has precedent because the design process prescribed in the IEC 61400–3 design standard endorses the derivation of a sea-based turbine design from the design of a land-based wind turbine.[23]

Ultimately, design modifications will have to be made to ensure that favorable performance is achieved and structural integrity is maintained for the wind turbine installed on the floating barge. Indeed, our loads analysis is just the first step in a design process that is, in actuality, an iterative process. And it is best to start with the simplest concept first (i.e., an onshore wind turbine mounted on top of an offshore barge) via the so-called "keep it simple, stupid" (KISS) principle. Nonetheless, by comparing the response of the floating system to the response of the turbine installed on land, we can we can quantify the impact brought about by the dynamic couplings between the turbine and floating barge in the presence of combined wind and wave loading. This comparison will point to the direction in which modifications must be made to arrive at a suitable design for the floating system. Such design modifications will have to be addressed through subsequent loads analysis iterations in later phases of the project.

We used the IEC 61400–1 design standard[22] for land-based turbines and the IEC 61400–3 design standard for sea-based turbines[23] as guides for our preliminary loads analysis. The –3 design standard is still in draft form and there are ongoing discussions concerning the design requirement prescriptions. Moreover, the –3 design standard explicitly states that "the design requirements specified in [the design] standard are not necessarily sufficient to ensure the engineering integrity of floating offshore wind turbines." However, for the purposes of our preliminary loads analysis, which is principally a feasibility study, we assumed that the stated design requirements were sufficient, and we made no attempt to identify other possible platform-specific design conditions.

A. Design Load Cases

Loads analysis involves verifying the structural integrity of a wind turbine by running a series of design load cases (DLCs) to determine the extreme (ultimate) and fatigue loads (i.e., forces and moments) expected over the lifetime of the machine and within the primary members of the wind turbine, including the blades, drivetrain, nacelle, tower, and for the floating system, mooring lines. The required DLCs cover essential design-driving situations such as normal operating conditions, start-up events, shut-down events, and parked or idling states, together with appropriate normal and extreme external conditions and likely fault scenarios.

Each IEC design standard prescribes numerous DLCs. It was not considered necessary for this preliminary loads analysis to run all the DLCs prescribed by the design standards; instead, we used a subset of the DLCs. Our biggest omission was to eliminate the fatigue-type DLCs and process only the anticipated ultimate loads. This omission follows from standard design practice for land-based and fixed-bottom sea-based wind turbines in which the structure is configured to survive ultimate loads before it is checked for fatigue.[38] Because fatigue behavior often governs the design of wind turbines however, we plan to assess the effect of platform motion on wind turbine fatigue damage by processing the omitted fatigue-type DLCs in a follow-on project.

The control system for the reference turbine does not include logic for startup or shutdown sequences, so we eliminated the 3.x, 4.x, and 5.x DLCs defined in the design standards (exception: we consider shutdowns that follow fault scenarios in DLC 2.x—see below). We also ignored the 8.x cases, which relate to transport, assembly, maintenance, and repair. These four DLCs may have governed the ultimate loading of some historical wind turbines, but we thought it was reasonable to omit them because, from our experience with land-based turbines, they have not dominated the ultimate loads.

The remaining ultimate-type DLCs included power production, DLC 1.x; power production with occurrence of fault, DLC 2.x; parked (idling), DLC 6.x; and parked with fault, DLC 7.x; design situations. We summarize the selected DLCs in Table 3. In this table, the DLCs are indicated for each design situation by their associated wind conditions, wave conditions, and operational behavior of the control system, fault scenarios, and other events. For the land-based cases, we disregarded the wave conditions and cantilevered the base of the tower to the ground. The wind and wave models are defined in Table 4 for readers who are unfamiliar with the IEC terminology.

In general, the –3 sea-based design standard is a superset of the –1 land-based design standard. When the two

Table 3. Summary of selected design load cases.

DLC	Winds		Waves			Controls / Events	Load
	Model	Speed	Model	Height	Direction		Factor
1) Power Production							
1.1	NTM	$V_{in} < V_{hub} < V_{out}$	NSS	$H_s = E[H_s\|V_{hub}]$	β = 0°	Normal operation	1.25*1.2
1.3	ETM	$V_{in} < V_{hub} < V_{out}$	NSS	$H_s = E[H_s\|V_{hub}]$	β = 0°	Normal operation	1.35
1.4	ECD	$V_{hub} = V_r$, V_r±2m/s	NSS	$H_s = E[H_s\|V_{hub}]$	β = 0°	Normal operation; ±Δ wind dir'n.	1.35
1.5	EWS	$V_{in} < V_{hub} < V_{out}$	NSS	$H_s = E[H_s\|V_{hub}]$	β = 0°	Normal operation; ±Δ ver. & hor. shr.	1.35
1.6a	NTM	$V_{in} < V_{hub} < V_{out}$	ESS	$H_s = 1.09*H_{s50}$	β = 0°	Normal operation	1.35
2) Power Production Plus Occurrence of Fault							
2.1	NTM	$V_{hub} = V_r$, V_{out}	NSS	$H_s = E[H_s\|V_{hub}]$	β = 0°	Pitch runaway → Shutdown	1.35
2.3	EOG	$V_{hub} = V_r$, V_r±2m/s, V_{out}	NSS	$H_s = E[H_s\|V_{hub}]$	β = 0°	Loss of load → Shutdown	1.10
6) Parked (Idling)							
6.1a	EWM	$V_{hub} = 0.95*V_{50}$	ESS	$H_s = 1.09*H_{s50}$	β = 0°, ±30°	Yaw = 0°, ±8°	1.35
6.2a	EWM	$V_{hub} = 0.95*V_{50}$	ESS	$H_s = 1.09*H_{s50}$	β = 0°, ±30°	Loss of grid → -180° < Yaw < 180°	1.10
6.3a	EWM	$V_{hub} = 0.95*V_1$	ESS	$H_s = 1.09*H_{s1}$	β = 0°, ±30°	Yaw = 0°, ±20°	1.35
7) Parked (Idling) and Fault							
7.1a	EWM	$V_{hub} = 0.95*V_1$	ESS	$H_s = 1.09*H_{s1}$	β = 0°, ±30°	Seized blade; Yaw = 0°, ±8°	1.10

Table 4. Definition of wind and wave models.

Abbr.	Definition	Description
ECD	Extreme Coherent Gust with Direction Change	This deterministic wind model consists of an unsheared gust superimposed on a uniform wind profile with a vertical power law shear exponent of 0.14. The gust rises to 15 m/s over a 10-s period. Occurring concurrently, the wind direction changes inversely proportional to the given hub-height wind speed. Both positive and negative direction changes are considered.
EOG	Extreme Operating Gust	This deterministic wind model consists of an unsheared gust superimposed on a uniform wind profile with a vertical power law shear exponent of 0.14. Over a 10.5-s transient, the gust first dips, rises to a maximum, then dips again before disappearing. Its magnitude depends on the wind turbine class (IB in this project) and increases with the given hub-height wind speed.
ESS	Extreme Sea State	This irregular sea state is similar to the NSS but uses a JONSWAP spectrum that is derived from 1- and 50-yr return values of the significant wave height and peak spectral period. Like the NSS, the sea state is modelled as a summation of sinusoidal wave components whose amplitude is determined by the wave spectrum, each parallel (long-crested) and described by Airy wave theory.
ETM	Extreme Turbulence Model	This model is similar to the NTM but consists of full-field 3-component stochastic winds with a higher turbulence standard deviation, which is based on the wind turbine class (IB in this project) and increases with the given hub-height wind speed. Like the NTM, the full-field turbulence is superimposed on a normal wind profile with a vertical power law shear exponent of 0.14.
EWM	Turbulent Extreme Wind Model	This model consists of full-field 3-component stochastic winds with a turbulence standard deviation of 0.11 times the 10-min average wind speed at hub-height, plus 0.2-m/s for 1-h long simulations. The full-field turbulence is superimposed on a wind profile with a vertical power law shear exponent of 0.11.
EWS	Extreme Wind Shear	This deterministic wind model consists of a linear shear superimposed on a uniform wind profile with a vertical power law shear exponent of 0.14. Over a 12-s transient, the shear rises to a maximum, then decreases again before disappearing. Its magnitude depends on the wind turbine turbulence category (B in this project) and increases with the given hub-height wind speed. Both positive and negative vertical and horizontal shears are considered independently.
NSS	Normal Sea State	This irregular sea state, representing stochastic waves, is modelled as a summation of sinusoidal wave components whose amplitude is determined by the wave spectrum, each parallel (long-crested) and described by Airy wave theory. The sea state is derived from the JONSWAP spectrum, whose formulation is based on the given values of the significant wave height and peak spectral period. The JONSWAP spectrum reduces down to the Pierson-Moskowitz spectrum in all but the most extreme sea states.
NTM	Normal Turbulence Model	This model consists of full-field 3-component stochastic winds with a turbulence standard deviation given by the 90% quantile, which is based on the wind turbine turbulence category (B in this project) and increases with the given hub-height wind speed. The full-field turbulence is superimposed on a wind profile with a vertical power law shear exponent of 0.14.

IEC design standards differed in details, we chose to use the specifications of the –3 design standard for both our land- and sea-based loads analyses. We wanted to use the same specifications for both analyses so that we could fairly compare the results. For example, the normal wind profile, used in both the deterministic and turbulent wind models, should consist of a vertical power law shear exponent of 0.2 for land-based wind turbines according to the –1 design standard and a value of 0.14 for sea-based turbines according to the –3 design standard. To facilitate the response comparisons, we decided to use 0.14 for both.

The –3 design standard specifies subsidiary cases for the DLCs involving extreme waves of 1- or 50-yr recurrence because it is, in general, difficult to account for both the irregularity and nonlinearity of the extreme waves simultaneously within simulation. This, in turn, follows from the fact that models for nonlinear irregular wave kinematics are not in common engineering usage. The subsidiary DLCs (a) involve analysis with turbulent winds and stochastic sea states used in conjunction with full system flexibility and dynamics, or (b and c) involve analysis with steady winds and deterministic nonlinear design waves used in conjunction with a quasi-steady computation with appropriate corrections for dynamic amplification. We chose the former method as indicated by the “a” in DLCs 1.6a, 6.1a, 6.2a, 6.3a, and 7.1a because it is not possible to model nonlinear waves in our simulation tool, which is based on the linearized radiation and diffraction method (see section II of this paper).

We ran all load case simulations for both the land- and sea-based turbine configurations using FAST[26] v6.10a-jmj with AeroDyn[27,28] v12.60i-pjm. We also reran some of the simulations in MSC.ADAMS® v2005.2.0 with A2AD[29,30] v12.21a-jmj and AeroDyn v12.60i-pjm to verify the responses predicted by FAST. (All results presented in this paper were produced by FAST, unless specified otherwise.) All simulations were run with all appropriate and available degrees-of-freedom (DOFs), including in FAST two flapwise and one edgewise mode DOFs per blade, one drivetrain torsion DOF, one variable generator-speed DOF, one nacelle yaw DOF, two fore-aft and two side-to-side tower mode DOFs, and for the floating system, three translational (surge, sway, and heave) and three rotational (roll, pitch, and yaw) DOFs of the platform. To account for manufacturing variability, all simulations also included a mass imbalance in the rotor, which instigates a once-per-rev excitation of the system when the rotor is spinning. The rotor mass imbalance was achieved by making one blade 0.5% heavier and one blade 0.5% lighter than the mass of the nominal (reference) blade. We did not model an aerodynamic imbalance (such as different blade pitch angles or twist distributions) because AeroDyn does not currently have that capability.

For the power production cases with and without faults, DLCs 1.x and 2.x, we used the quasi-steady, blade-element/momentum (BEM) axial induction model with the Beddoes-Leishman dynamic stall model in AeroDyn. We chose the BEM induction model over AeroDyn's generalized dynamic wake induction model (GDW) because the GDW model is not suitable when the turbulent wake state is approached (particularly at low wind speeds),[28] and we did not wish to see a change in response at the wind speed where we would have had to switch between the different models. Likewise, we chose the axial induction model over AeroDyn's option for a combination of axial and tangential (rotational) induction models because the tangential induction model is not numerically stable at all rotor speeds under consideration (particularly the low rotor speeds during a shutdown event). Moreover, we disabled both the BEM induction model and the dynamic stall model in AeroDyn for DLCs 6.x and 7.1a, relying instead on simple table-lookup aerodynamics with geometric angles-of-attack, because the BEM and dynamic stall models are not applicable in parked (idling) cases (particularly at the very high post-stall angles-of-attack).

The generator torque and blade pitch control systems are operating properly and the turbine is producing power normally in DLCs 1.x and prior to the fault in DLCs 2.x. The control system is disabled in DLCs 6.x and 7.x. Instead, the rotor is idling in these DLCs with no generator or brake reaction torques and all blades fully-feathered to the maximum pitch setting of 90º (exception: one blade is seized at the minimum set point in DLC 7.1a—see the next paragraph). The control system for the 5-MW baseline wind turbine does not include logic for the active control of nacelle yaw. So in all DLCs, we secured the nacelle at given yaw angles with a spring and damper to represent compliance in the yaw drive. We describe the given yaw angles when discussing wind conditions below.

For DLCs 2.x and 7.x that involve fault conditions, the IEC design standards require that faults with the worst consequences be chosen. We chose common design-driving faults based on our experience with other land-based wind turbine loads analyses. For DLC 2.1, we simulated a fault in the collective blade-pitch control system where one blade ignores its command and runs away to the minimum set point of 0º at the full pitch rate of 8º/s. We assume that the turbine's protection system detects this fault in this situation by simulating a shut down of the turbine; the shut down is initiated after a 0.2-s delay (to account for the time it takes the protection system to detect the fault and take action) by feathering the other two blades at full pitch rate to the maximum pitch setting of 90º. For DLC 2.3, we simulated a fault where the load is lost, implying that the generator reaction torque is zero. In this situation, we again assume that the turbine's protection system detects the fault and shuts down the turbine by feathering all blades after a 0.2-s delay at full pitch rate to the maximum pitch setting. For DLC 7.1a, we simulated the fault condition where one blade is seized at the minimum set point (i.e., flat into the wind) while idling with the other two blades fully feathered.

The hub-height wind speeds, V_{hub}, considered within each DLC are listed in Table 3. In the turbulent wind models (ETM, EWM, and NTM), V_{hub} represents the average hub-height wind speed over a simulation. In the deterministic wind models (ECD, EOG, and ECD), V_{hub} represents the steady wind speed at hub-height in the absence of the transient gust. For the cases where a wind speed range is indicated from cut-in to cut-out, $V_{in} < V_{hub} < V_{out}$, we used a set of simulations with discrete values of V_{hub} centered within bins of 2 m/s width (i.e., discrete values of 4, 6, …, 24 m/s). This resolution came from guidance in the IEC design standards. Even though the design standards recommend that DLC 2.1 be analyzed at all wind speeds between cut-in and cut-out, we chose to analyze this load case only at the rated, V_r, and cut-out, V_{out}, wind speeds, again based on our experience that they produce the highest loads. The extreme wind conditions were considered with the 1- and 50-yr recurrence values of the mean reference hub-height wind speed, V_1 and V_{50}, respectively, as shown in Table 3.

We generated the turbulent full-field 3-component wind conditions with TurbSim[32] v1.20. We used the Kaimal wind spectrum because TurbSim does not have the capability of generating turbulent wind-inflow with the IEC-recommended[22] Mann model. We generated the deterministic wind conditions with a customized copy of

IECWind[33] v5.00. We had to customize IECWind so that it would generate wind-inflow with a vertical power-law shear exponent of 0.14 because it was originally developed only for the –1 design standard.

All winds were generated with a mean wind direction and a vertical inclination of the mean flow angle of 0º, except in DLC 1.4 where the wind direction departs from 0º during the gust. A mean wind direction of 0º implies in our simulations that the rotor is aligned properly with the wind when the platform and nacelle are not displaced. For the power production cases with and without faults, we aligned the rotor with the wind at the start of the simulation by securing the nacelle yaw angle at 0º. For the parked (idling) cases, we also included nonzero-mean yaw misalignments as directed by the design standards and indicated by the yaw specifications in Table 3. DLC 6.2a considers the full range of yaw misalignments, -180º < Yaw < 180º, because of an assumed inability of the yaw controller to align the rotor with the wind during a situation in which electrical power is unavailable while the grid is lost. To cover the range of yaw misalignments in this case, we used a set of simulations with discrete yaw angles in increments of 20° (i.e., discrete values of -160º, -140º, …, 180º).

Per the guidance of the –3 design standard and as shown in Table 3, all normal wave conditions (NSS), involving irregular sea states, were considered with a significant wave height, H_s, given by the expected value conditioned on the relevant mean hub-height wind speed, $E[H_s,V_{hub}]$, based on the long-term joint probability distribution of metocean parameters at our reference site (see section III.C). The range of peak spectral periods associated with each expected significant wave height, T_p, was split uniformly into three bins and was considered in our loads analysis by running three sets of simulations with discrete values of T_p centered within those bins. The extreme stochastic sea states (ESS) were considered with the 1- or 50-yr recurrence values of the significant wave height, H_{s1} and H_{s50}, respectively. We used H_{s50} as a conservative estimate for the severe 50-yr significant wave heights conditioned on the relevant mean hub-height wind speeds in DLC 1.6a. We did this because we did not have the opportunity to compute the later values, which must be determined by extrapolation of the appropriate site-specific metocean data such that the combination of the significant wave height and wind speed has a recurrence period of 50 years. This practice again follows the guidance of the –3 design standard. As in the normal wind conditions, we ran three sets of simulations with discrete values of T_p in the extreme sea states to represent the range of wave peak spectral periods associated with H_{s1}. But in the simulations with extreme sea states using H_{s50}, we only used one value of T_p (the midpoint in the range) because there was only a very small range of associated peak spectral periods in the reference site data. The waves were considered to propagate co-directionally with the winds in DLCs 1.x and 2.x, $\beta = 0$ º, except in DLC 1.4 where the wind direction departs from the wave direction during the gust. For the parked (idling) cases, we also included wave misalignments as directed by the –3 design standard and indicated by the β specifications in Table 3. The design standard requires one to consider wind and wave misalignments of up to 30° before reducing the severity of the sea state, so in DLCs 6.x and 7.1a we considered three wave heading directions, one aligned with the wind and two misaligned with the wind by ±30°.

The design standards specify the minimum quantity and length of each simulation in each load case. More than one simulation is required for each pair of turbulent wind and stochastic wave conditions to obtain statistically reliable results. The simulations at each pair of turbulent wind and stochastic wave conditions are differentiated through the choice of varying seeds in their respective pseudo-random number generators. We paired our wind and wave seeds so that when n seeds were required, we ran n total simulations instead of all n^2 combinations of the two seeds.

For DLCs 1.1 and 1.3, the –3 design standard requires that six 10-min simulations be run at each wind and wave condition, differentiated with variations in the wind and wave seeds. For DLCs 1.4 and 1.5, the design standard requires six 1-min simulations at each wind and wave condition, differentiated with variations in the wave seed (the deterministic wind models do not require the specification of random seeds). For DLC 2.1, the design standard requires twelve 10-min simulations at each wind and wave condition, differentiated with variations in the wind and wave seeds. For DLC 2.3, the design standard requires six 1-min simulations at each wind and wave condition, differentiated with variations in the wave seed and the time at which the load is lost relative to the gust. Finally, for cases with extreme sea states, DLCs 1.6a, 6.x, and 7.1a, the design standard requires six 1-h simulations at each wind, wave, and nacelle yaw condition, differentiated with variations in the wind and wave seeds. In this last group of DLCs, a factor of 1.09 is needed to scale the 1- and 50-yr recurrence significant wave heights corresponding to a 3-h reference period to the 1-h length of the simulation. Likewise, a factor of 0.95 is needed to scale the 1- and 50-yr recurrence values of the 10-min average wind speeds to the 1-h length of the simulation. These scale factors also come from the –3 design standard.

For the power production cases with and without faults, we initialized the rotor speed and blade pitch angles based on the given mean hub-height wind speed for each simulation to mitigate the start-up transient behavior, which is an artifact of the computational analysis. We initialized the rotor speed and blade pitch angles to the values they would trim to, based on the action of the control system, if the given wind speeds were steady and uniform.

Nevertheless, we added 30 s to the required simulation times stated above before outputting simulation data to eliminate any remaining start-up transient behavior that may have spuriously affected our loads predictions. So we actually ran the 1-min simulations for 90 s, etc. All of the transient gusts, shears, and direction changes in the deterministic wind models were initiated 60 s into the simulation (i.e., 30 s after the end of the 30-s start-up transient). Likewise, the blade-pitch control system faults in DLC 2.1 were initiated 60-s into the simulation. The loss of load in DLC 2.3 was initiated at varying times during the 10.5-s gust, depending on the random seed as indicated in the previous paragraph.

Accounting for all of the combinations of wind conditions, wave conditions, and control scenarios, together with the number of required seeds, we ran a total of 2,190 separate sea-based simulations and 452 separate land-based simulations in our loads analysis. To manage the quantity and variety of simulations, we developed and utilized custom-made scripts written in Perl and the Windows batch command language. Using scripts greatly reduced the chance of mistakes (and eliminated a great deal of tedium). The main Perl script used an input file to specify which of the aforementioned DLCs would be run and with what specific parameters. This script was developed to process all of the cases sequentially on one computer, or in parallel using the job-queuing utility known as Condor,[†††] which permits one to distribute a set of simulations between all idle computers on a network. We used the former only for debugging. Using Condor on the 45 to 60 processors we had available to us enabled us to run most of the DLC simulations overnight. If we had to run them all sequentially on a single computer, it would have taken just over three weeks of processing time per loads analysis!

B. Post Processing and Partial Safety Factors

Besides examining the time-series output from simulations, we processed all of the loads analysis data using the post-processing computer program Crunch[39] v3.00.00, called with another custom-made Windows batch script. We processed each DLC in separate Crunch runs because the processing requirements varied by DLC and because Crunch is limited to processing files of all the same length in a given run. We also had memory restrictions and had to run Crunch on a 64-bit server with 16 GB of RAM to hold the biggest DLC dataset in memory all at the same time. We processed the loads data with Crunch in two different ways. First, we had Crunch compute the statistics (i.e., minimum, mean, and maximum value, standard deviation, skewness, etc.) of each output parameter for each simulation in each DLC. These data enabled us to characterize the dynamic response of the land- and sea-based systems under the influence of the wind conditions, wave conditions, and control scenarios pertinent to each DLC. Second, we had Crunch generate extreme-event tables for each DLC. These tables list the extreme minimum and maximum loads for a group of similar output parameters, along with the associated values of the other parameters that occur when the extreme load is reached. The tables also list the specific simulation that triggered the extreme loads and the times at which they occurred, as well other information that may be relevant to the event, such as instantaneous hub-height wind speed and wave elevation.

As Crunch read in the simulation output for the extreme-event processing, we had it apply partial safety factors (PSFs) to the blade tip-to-tower clearance outputs, to the internal loads in the wind turbine, and for the floating system, to the tensions in the mooring lines. We did not apply the PSFs to other output parameters, including the blade tip and tower-top deflections, the floating platform displacements, and the control actions such as the generator torque and power output, and blade pitch angles. The PSFs for loads, as specified in the IEC design standards, varied by DLC, and we document them in the last column of Table 3. In addition, an extra factor of 1.2 is stated for DLC 1.1. The IEC design standards require that the ultimate loads predicted under normal operation with normal wind turbulence and stochastic wave conditions be based on the statistical extrapolation of the load response. To eliminate this extra step, we decided to use a rule of thumb resulting from experience with other loads analysis exercises. From our and others experiences, the extrapolation typically increases the predicted ultimate load by 20%. This factor is further justified by the example extrapolation given in Appendix F of the –1 design standard.[22] So we increased the normal 1.25 load PSF for DLC 1.1 by 20%, to a value of 1.5. However, we did not increase the load PSF by 20% for the calculation of the blade tip-to-tower clearance outputs in DLC 1.1 as per the design standard, which says that one should not extrapolate deflections.

The PSFs for loads "take account of possible unfavorable deviations/uncertainties of the load from the characteristic value [and] uncertainties in the loading model."[22] We applied the PSFs to the loads in our extreme-event processing to enable a useful comparison of the loads between the DLCs. That is, it is necessary to weight each DLC properly when determining the DLC that causes the overall ultimate (maximum) load because loads from abnormal design situations, which are less likely to occur, should be given a lower weighting (and are given a lower load PSF) than normal more commonly-occurring loads. To get the global extremes across all DLCs, we combined

[†††] Website: http://www.cs.wisc.edu/condor/.

all of the extreme-event tables from each DLC using a slightly-customized copy of the Perl script CombEEv v1.20.[40] We had to customize CombEEv so that it would not only generate the global extreme-event tables, but also the absolute extremes for each output parameter (i.e., the absolute maximum value of the minimums and maximums). We used the absolute extremes for each output parameter to compare the land- and sea-based loads results.

The IEC design standards also document PSFs for materials and consequences of failure. We did not apply these, however, because they are the same across all load cases and will thus cancel out in the comparison and because we made no attempt to compare the load predictions to the material or buckling strengths of the individual components.

V. Loads Analysis Results and Discussion

We ran loads analyses for extreme (ultimate) loads using the simulation capability documented in section II, the properties of the wind turbine, floating barge, and reference site described in section III, and the load case conditions and procedures explained in section IV of this paper. We now present the results of this analysis. Due to the shear quantity of results, which includes over 100 GB of data, we cannot present them all in this paper. Instead, we focus on results that are characteristic of the overall system responses.

Not to ruin the surprise, but our loads analysis helped identify design problems with both the land- and sea-based system configurations. We discovered a side-to-side instability in the tower of the idling land-based wind turbine in DLC 6.2a. In the sea-based system, we discovered an instability in the yaw motion of the floating platform that manifested itself in the fault conditions of DLCs 2.1 and 7.1a. Finally, we determined that the floating barge system is susceptible to excessive platform pitching motion in large and/or steep waves, especially in extreme waves, such as those occurring during 1- and 50-yr events in DLCs 1.6a, 6.x, and 7.1a. The end result of these design problems is that they all led to unreasonable loading of the wind turbine, which dominated the final predictions in ultimate loads.

To provide insight into the dynamic behavior of the onshore and floating systems, and to enable a fair comparison between the two, the results are split into groups and presented separately. In section V.A, we present the land- and sea-based results for DLCs 1.1, 1.3, 1.4, and 1.5, which consider the wind turbine in normal operation with a variety of external wind and wave conditions, not including extreme 1- or 50-yr events. These results embody the response of the systems unencumbered by the abovementioned design problems. We then present in section V.B our findings from the other load cases, DLCs 1.6a, 2.x, 6.x, and 7.1a, which are concerned with the wind turbine when it is experiencing a fault, when it is idling, and/or when it is being excited by 1- and 50-yr wind and wave conditions. Our presentation of this later group of DLCs includes a description of the ensuing design problems and possible mitigation measures.

A. Normal Operation

We processed the loads analysis results from the normal operation cases to characterize the dynamic response of the land- and sea-based systems, to identify the design-driving conditions and to quantify the resulting ultimate loads, and to measure the impact of installing the wind turbine on the ITI Energy barge.

1. Characterization of the Dynamic Response

Figure 7 presents the minimum, mean, and maximum values from each simulation in DLC 1.1 for several output parameters. These values are not scaled by the PSFs for loads described in section IV.B. The statistics from both the land- and sea-based systems are presented side-by-side. The results for the floating system are further grouped by the peak spectral period of the incident waves in each sea state.

The mean values (indicated by the middle dots) of all parameters are very similar between land and sea, except for the mean value of the platform pitch, which is zero for the land-based wind turbine because its tower is cantilevered to the ground at its base. As planned, the mean value of the rotor speed increases linearly with mean hub-height wind speed below rated (11.4 m/s) to maintain constant tip speed ratio and optimal wind power conversion efficiency. Likewise, the mean generator power and rotor torque increase dramatically with wind speed up to rated, increasing cubically and quadratically, respectively. Above rated, the mean generator power is held constant by regulating to a fixed speed with active blade pitch control and a generator torque that is inversely proportional to the generator speed. The mean values of the out-of-plane tip deflection and root bending moment of the reference blade (blade 1) reach a maximum at rated before dropping again. This response characteristic is the result of a peak in rotor thrust at rated (not shown). This peak is typical of variable speed, variable pitch-to-feather wind turbines due to the transition that occurs in the control system at rated between the active generator torque and the active blade pitch control regions. This peak in response is also visible, though less pronounced, in the mean values of the platform pitch, tower-top fore-aft deflection, and tower-base fore-aft bending moments.

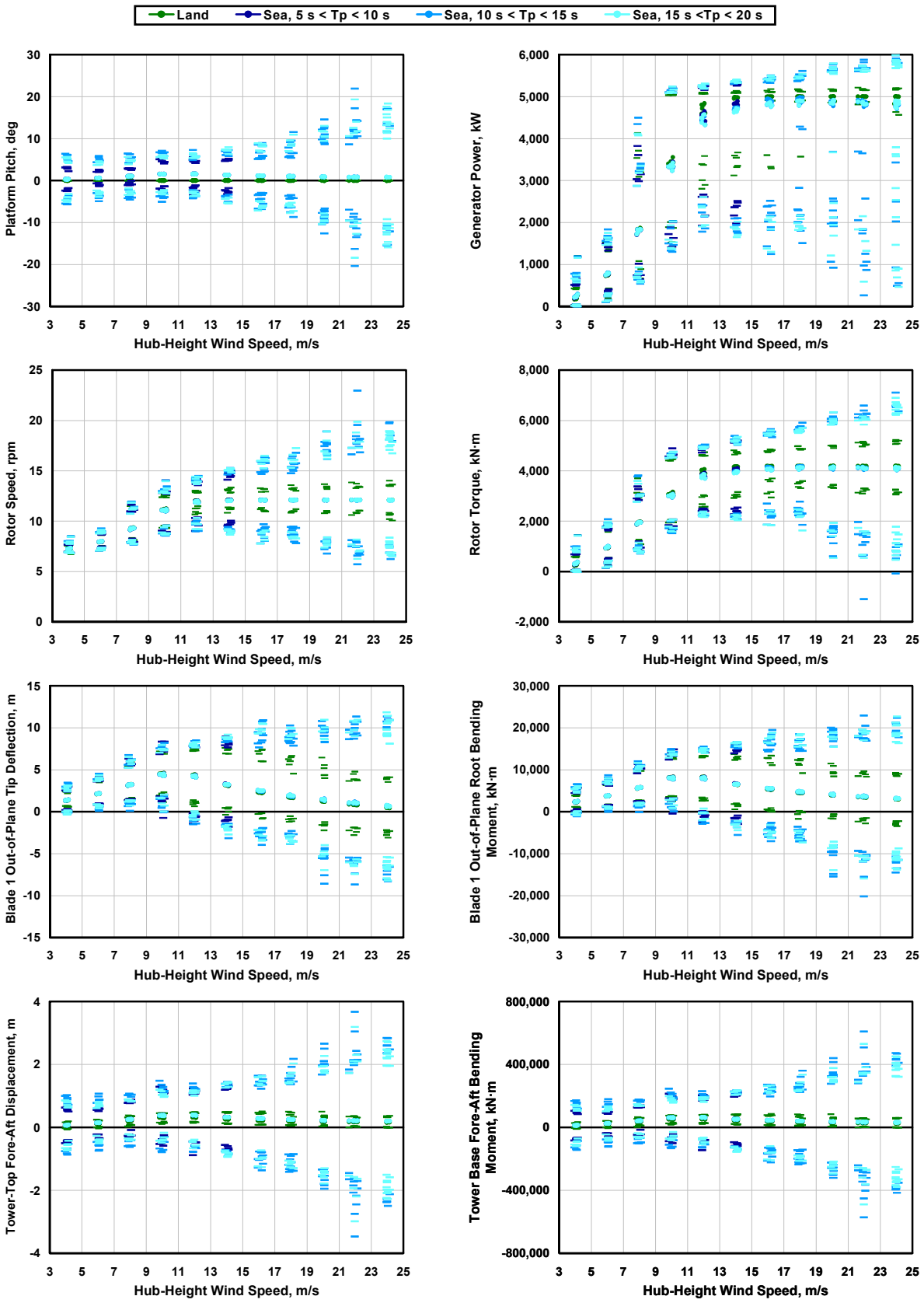

Figure 7. Minimum, mean, and maximum values from each simulation in DLC 1.1.

The mean values are similar between land and sea, but Fig. 7 shows that the excursions of the minimum and maximum values (indicated by the lower and upper horizontal dashes, respectively) in the sea-based results are much larger. Due to the weak authority of the blade-pitch control system to regulate speed when operating near optimal wind power conversion efficiency, the widest spread between the minimum and maximum values in the land-based simulations occurs in the generator power parameter just above rated. The excursions of minimum and maximum values for all parameters in the sea-based simulations, however, increase with wind speed. More precisely, they increase with the pitch motion of the floating platform, which increases with wind speed because the barge has a natural tendency to move with surface waves, and because the expected value of the significant wave height increases with wind speed as shown in section III.C. The pitching of the barge causes large variations in the generator power and rotor speed, which may lead to a loss of energy capture and an increase in aeroacoustic emissions. The pitching of the barge also causes large load excursions, more so for the tower base loads than for the loads in the blades and drivetrain because the floating system acts as an inverted pendulum, with the largest effect from inertia loading nearest the pivot point. The minimum and maximum loads in the floating system are worst with sea states derived from large significant wave heights and from peak spectral periods in the range of 10 to 15 s. The wave period range of 10 to 15 s is particularly dominate since the resulting waves are more likely to excite the rigid-body turbine plus barge pitch mode, which has a natural frequency of about 0.086 Hz, and which equates to a natural period of 11.6 s. So even though the expected significant wave height is lower at a mean hub-height wind speed of 22 m/s than at 24 m/s, the loads in the floating system are higher at 22 m/s than at 24 m/s, where the wave periods are higher.

Similar trends in statistics exist for both the land-and sea-based system responses in DLC 1.3 (not shown). The only difference is that some of the output parameters, particularly for the land-based wind turbine, have slightly larger load excursions due to the increased turbulence in the wind-inflow.

2. Identification of Design-Driving Load Cases and Quantification of Ultimate Loads

We identified the design-driving load conditions and quantified the resulting ultimate loads by generating extreme-event tables. We created 21 tables for the land-based loads and 32 tables for the sea-based loads (we don't show them all in this paper). Each table contains a distinct group of similar output parameters, such as the internal loads in the blades, drivetrain, nacelle, and tower, and for the floating system, tensions in the mooring lines. The extreme-events for the root moments of the reference blade (blade 1) in the land- and sea-based analyses are presented in Tables 5 and 6, respectively. Likewise, the extreme-events for the tower base moments in the land- and sea-based analyses are presented in Tables 7 and 8, respectively.

The extreme-events tables record the extreme minimum and maximum loads (the shaded values on the diagonal) for each parameter (identified in the first column), the name of the simulation output file that triggered the extreme load (third column), the time at which the extreme load was reached (last column), and the associated values of the other parameters that occur when the extreme load is reached (off-diagonal values). The loads data have all been weighted using the PSFs for loads described in section IV.B. In an actual turbine design, these loads data would be fed into an FEA program to determine the detailed stress distributions within individual turbine components, such as the blades, hub, shaft, and tower. We did not perform this extra step, however, because our project is only a conceptual and feasibility study.

In the parameter names for the blade-root moment tables, "Mxc1," "Myc1," and "Mzc1" refer to the internal

Table 5. Extreme-events for the blade 1 root moments – land.

Parameter	Type	File	RootMxc1 (kN-m)	RootMyc1 (kN-m)	RootMzc1 (kN-m)	Time (sec)
RootMxc1	Min	DLC1.3_0063_Land_24.0V0_S03.out	-7.48E+03	-2.13E+03	-1.68E+02	5.99E+02
RootMxc1	Max	DLC1.1_0061_Land_24.0V0_S01.out	1.11E+04	1.15E+04	-1.11E+02	5.66E+02
RootMyc1	Min	DLC1.4_0006_Land_ECD-R+20.out	1.93E+03	-6.81E+03	-2.24E+02	6.92E+01
RootMyc1	Max	DLC1.4_0002_Land_ECD+R.out	-7.78E+02	2.22E+04	1.18E+02	7.90E+01
RootMzc1	Min	DLC1.4_0006_Land_ECD-R+20.out	-1.75E+02	-5.18E+03	-2.81E+02	6.88E+01
RootMzc1	Max	DLC1.3_0038_Land_16.0V0_S02.out	-2.00E+03	1.77E+04	2.11E+02	1.53E+02

Table 6. Extreme-events for the blade 1 root moments – sea.

Parameter	Type	File	RootMxc1 (kN-m)	RootMyc1 (kN-m)	RootMzc1 (kN-m)	Time (sec)
RootMxc1	Min	DLC1.1_0149_Sea_20.0V0_04.4Hs_14.1Tp_S02.out	-1.21E+04	-1.28E+04	-2.26E+02	1.96E+02
RootMxc1	Max	DLC1.1_0190_Sea_24.0V0_05.5Hs_12.7Tp_S04.out	1.55E+04	1.66E+04	-1.43E+02	5.92E+02
RootMyc1	Min	DLC1.1_0164_Sea_22.0V0_04.7Hs_13.4Tp_S01.out	7.43E+03	-3.03E+04	6.87E+02	2.60E+02
RootMyc1	Max	DLC1.1_0164_Sea_22.0V0_04.7Hs_13.4Tp_S01.out	4.72E+03	3.43E+04	3.15E+02	2.56E+02
RootMzc1	Min	DLC1.4_0030_Sea_ECD+R_02.4Hs_17.6Tp_S04.out	-2.14E+03	-8.11E+03	-4.70E+02	8.80E+01
RootMzc1	Max	DLC1.1_0164_Sea_22.0V0_04.7Hs_13.4Tp_S01.out	7.21E+03	-2.99E+04	7.21E+02	2.60E+02

Table 7. Extreme-events for the tower base moments – land.

Parameter	Type	File	TwrBsMxt (kN-m)	TwrBsMyt (kN-m)	TwrBsMzt (kN-m)	Time (sec)
TwrBsMxt	Min	DLC1.3_0057_Land_22.0V0_S03.out	-2.77E+04	2.78E+04	-8.14E+02	4.83E+02
TwrBsMxt	Max	DLC1.3_0064_Land_24.0V0_S04.out	4.09E+04	2.64E+04	1.83E+03	9.16E+01
TwrBsMyt	Min	DLC1.3_0004_Land_04.0V0_S04.out	-4.77E+03	-3.53E+04	1.58E+03	3.40E+02
TwrBsMyt	Max	DLC1.3_0051_Land_20.0V0_S03.out	9.04E+03	1.53E+05	1.49E+03	1.19E+02
TwrBsMzt	Min	DLC1.3_0062_Land_24.0V0_S02.out	2.63E+03	4.45E+04	-1.23E+04	5.62E+02
TwrBsMzt	Max	DLC1.3_0063_Land_24.0V0_S03.out	4.90E+03	3.02E+04	1.20E+04	5.99E+02

Table 8. Extreme-events for the tower base moments – sea.

Parameter	Type	File	TwrBsMxt (kN-m)	TwrBsMyt (kN-m)	TwrBsMzt (kN-m)	Time (sec)
TwrBsMxt	Min	DLC1.1_0182_Sea_24.0V0_05.5Hs_15.5Tp_S01.out	-1.99E+05	-1.21E+05	5.70E+02	6.11E+02
TwrBsMxt	Max	DLC1.1_0182_Sea_24.0V0_05.5Hs_15.5Tp_S01.out	2.15E+05	3.12E+05	-9.88E+03	6.17E+02
TwrBsMyt	Min	DLC1.1_0164_Sea_22.0V0_04.7Hs_13.4Tp_S01.out	7.71E+04	-8.58E+05	1.25E+04	2.62E+02
TwrBsMyt	Max	DLC1.1_0164_Sea_22.0V0_04.7Hs_13.4Tp_S01.out	2.75E+04	9.14E+05	1.24E+04	2.56E+02
TwrBsMzt	Min	DLC1.4_0026_Sea_ECD+R_02.4Hs_13.4Tp_S03.out	-6.40E+03	-1.85E+04	-2.16E+04	8.33E+01
TwrBsMzt	Max	DLC1.3_0164_Sea_22.0V0_04.7Hs_13.4Tp_S01.out	9.02E+04	-6.21E+05	2.15E+04	2.63E+02

moments about the x-, y-, and z-axes of the coordinate system of blade 1, which is fixed in the hub so as not to rotate with the pitch control motion of the blade. The x-axis of this coordinate system is directed nominally downwind, the y-axis is located in the plane of rotation, and the z-axis is directed from the hub to the tip of blade 1. Thus, the parameters correspond to the in-plane bending moment, the out-of-plane bending moment, and the pitching (torsion) moment at the root of blade 1, respectively. In the parameter names for the tower base, "Mxt," "Myt," and "Mzt" refer to the internal moments about the x-, y-, and z-axes of the tower-base coordinate system. The x-axis of this coordinate system is directed nominally downwind, the y-axis is directed transverse to the nominal wind direction, and the z-axis is directed vertically from the tower base to the yaw bearing. Thus, the parameters correspond to the roll (side-to-side) bending moment, the pitch (fore-aft) bending moment, and the yaw (torsion) moment at the tower base, respectively. The file names list the DLC, the simulation number, the land- or sea-basis, the wind and wave conditions, and the random seed identifier.

For the wind turbine installed on land, Table 5 shows that DLCs 1.3 and 1.4 drive most of the extreme root moments in blade 1 and Table 7 shows that DLC 1.3 produces all of the extreme moments in the base of the tower. In contrast, Tables 6 and 8 show that DLC 1.1 plays more of a roll at triggering the ultimate loads for the wind turbine mounted on the barge. In particular, the sea-based simulation in DLC 1.1 numbered 164 generates (a) the minimum and maximum out-of-plane bending moments in the root of blade 1, (b) the maximum pitching moment in the root of blade 1, (c) the minimum and maximum pitch bending moments in the tower base, and (d) the maximum yaw moment in the tower base—all within a 7 s period of time (i.e., from time 256 to 263 s)!

3. Description of Design-Driving Load Events

To determine the exact sequence of events and the physics behind the dynamic response that led to the extreme load of each output parameter, we examined the time series output from each of the dominant simulations identified by the extreme-events tables.

Figure 8 presents a portion of the time series for several output parameters from the sea-based simulation in DLC 1.1 numbered 164. Results from independent FAST and ADAMS runs are shown side-by-side. As indicated within the associated file name in Tables 6 and 8, this particular simulation has a random seed identifier of 1, stochastic winds with a mean hub-height wind speed of 22 m/s, and irregular waves with a significant wave height of 4.7 m and a peak spectral period of 13.4 s.

Of the parameter names in Fig. 8 not previously defined, "WindVxi" represents the instantaneous nominally downwind component of the wind speed at hub-height, "WaveElev" represents the instantaneous wave elevation relative to the still water level at the origin of the undisplaced platform, "PtfmPitch" represents the instantaneous pitch angle of the platform (barge), "GenPwr" represents the instantaneous electrical output of the generator, "RotSpeed" represents the instantaneous rotational speed of the rotor, and "RotTorq" represents the instantaneous mechanical torque in the low-speed shaft.

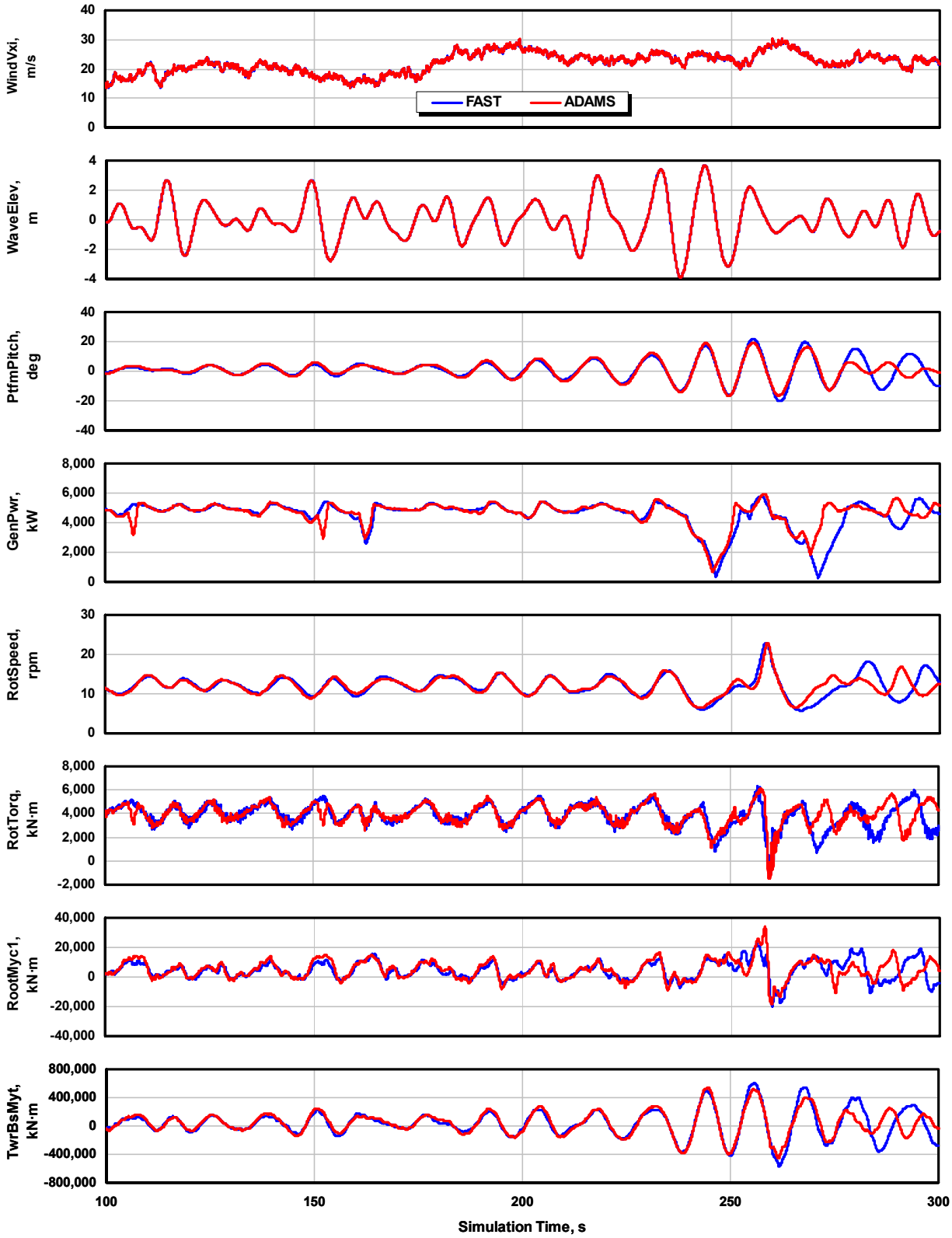

Figure 8. Time series system response from the sea-based simulation in DLC 1.1 numbered 164.

The response of the floating system during the first half of the time series in Fig. 8 is characteristic of its response in many other simulations. The incident waves cause the barge to pitch back and forth. The ensuing motion in the supported wind turbine causes all of the other parameters to exhibit the same oscillatory behavior. Moreover, the pitching causes a large translation of the wind turbine's nacelle, which results in an oscillating inflow to the rotor. As the platform pitches downwind (positive slope), the rotor's relative wind speed decreases, which causes the applied aerodynamic torque to drop and the control system responds by driving the blade pitch angles to zero (not shown). As the aerodynamic torque drops, there is a mismatch with the generator torque, so the rotor speed decreases as well. The rotor speed exhibits much more variation than one would see in a land-based wind turbine. (The rotor torque shown in Fig. 8 equals the difference between the applied aerodynamic torque and the rotor inertia acceleration or deceleration by d'Alembert's principle,[41] which is why the phase of the response may not follow intuition.)

During the second half of the time series in Fig. 8, the response of the floating system changes considerably. As shown, a series of large incident waves begins to impinge upon the barge. These waves have a height of around 7 m and propagate near the barge pitch natural frequency of 0.086 Hz. Concurrent with these waves are sustained hub-height winds near cut-out (25 m/s) that are then followed by a gust to 30 m/s. These wind and wave conditions bring about excessive pitch motion of the barge that leads to large loads in the blades and tower, large excursions in the rotor speed and generator power output, as well as extreme values in the rotor thrust, tower-top displacement, and nacelle acceleration output-parameters (not all shown). In fact, this one series of events drives one-quarter of the extreme values for all of the most relevant output parameters. The loads plotted in this figure are not scaled by the PSFs, which is why the extreme values of the blade root out-of-plane and tower-base pitch bending moments that may be spotted from the FAST time series do not exactly match the values listed in the extreme-events tables shown earlier.

There are differences between the FAST and ADAMS predictions in Fig. 8, mostly after the series of events that trigger the largest loads. We believe these differences are caused by the greater structural fidelity of the ADAMS simulator, which includes torsion and mass offsets in the blade model that are not accounted for in FAST. A clear consequence of these differences is that the blade pitch angles are smaller for ADAMS than for FAST because the control system in FAST must compensate for the lack of blade twist. This difference is visible in the simulation results we present next.

By examining Table 5 and other extreme-events tables not presented in this paper, we discovered that DLC 1.4 drives the extreme out-of-plane blade tip deflections and several blade loads in both the land- and sea-based system configurations. Figure 9 presents a portion of the time series for several output parameters during the sea-based simulation of this design-driving event. Again, results from independent FAST and ADAMS runs are shown side-by-side and the data are not scaled by the PSFs for loads. Of the parameter names not previously defined, "BlPitch1" represents the instantaneous pitch angle of blade 1, "OoPDefl1" and "IPDefl1" represent the instantaneous out-of-plane and in-plane tip deflections of blade 1 relative to the undeflected pitch axis, "NcIMUTAxs" represents the instantaneous acceleration of the inertial measurement unit, which is located in the nacelle at, and aligned with the centerline of, the main low-speed shaft bearing, and "PtfmYaw" represents the instantaneous yaw angle of the platform (barge).

This particular simulation is numbered 101 and has a random seed identifier of 4, a steady hub-height wind speed of 13.4 m/s (2 m/s above rated) before the ECD event, and irregular waves with a significant wave height of 2.7 m and a peak spectral period of 12.7 s. Before the ECD event, which started at 60 s, the barge oscillates in pitch, due again to the impinging surface waves. This is seen in Fig. 9 through its oscillatory effect on the out-of-plane blade tip deflection and root bending moment, the nacelle fore-aft acceleration, the rotor speed, and the blade pitch angle. The blade pitch angle varies due to the action of the control system in response to the oscillating rotor speed, which in turn, results from the oscillating wind-inflow relative to the rotor as described above. So interestingly, even when the hub-height wind speed is above rated and steady, there are still short periods of below rated operation where power is lost.

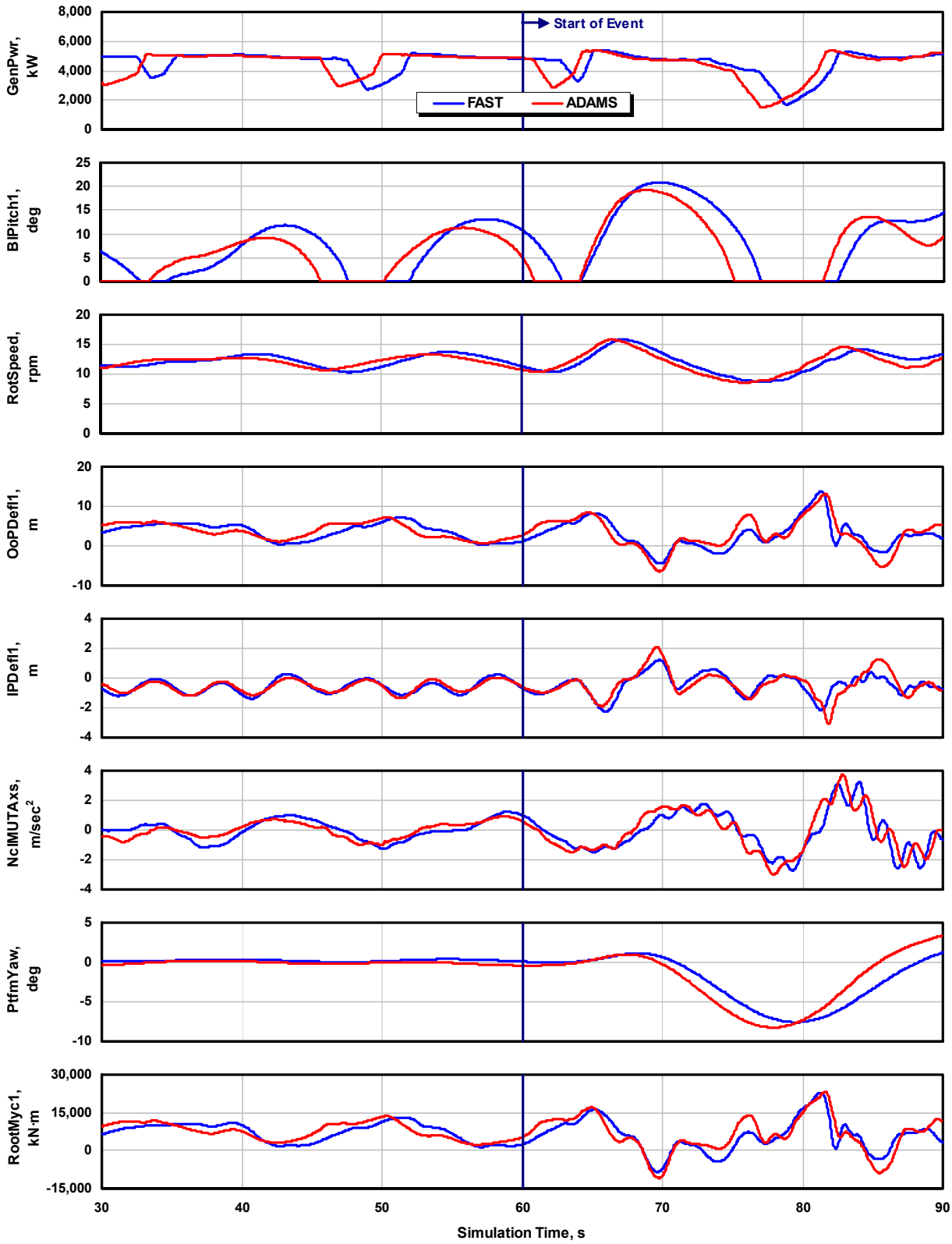

Figure 9. Time series system response from the sea-based simulation in DLC 1.4 numbered 101.

The ECD event started at 60 s and took 10 s to reach the 15-m/s increase in wind speed and the concurrent 54º change in wind direction. The wind direction shifted to the left when looking downwind. As shown in Fig. 9, the escalation in wind speed from the gust generates a rise in the rotor speed and an increase in the blade pitch angle as the control system tries to compensate. But the wind direction change produces a large nacelle yaw error that causes the wind speed relative to the rotor to eventually drop, which in turn causes the rotor speed and blade pitch angle to decrease. The maximum out-of-plane tip deflection (of nearly 14 m!) occurs after this series of events, when the blade is pointing horizontally into the wind just after the blade pitch angle reaches its 0º minimum set point. This condition is worst for the blade because the blade is flat into the wind during that time. Although the extreme out-of-plane bending moment at the root of blade 1 is higher in DLC 1.1, this series of events in DLC 1.4 brings about the maximum out-of-plane bending moment in blade 1 at 50% span (not shown in Fig. 9). The ECD event also perturbs the yaw angle of the barge. After the event is over, the barge begins to yaw slightly into the wind. There is still about a 50º nacelle yaw error at 90 s into the simulation, but the mooring lines eventually restrain the platform from yawing any farther.

Of all the different hub-height wind speeds we ran simulations for in DLC 1.4, the simulations we ran at a wind speed of 2 m/s above rated led to the largest out-of-plane tip deflections in the floating turbine because this wind speed was associated with the highest wave heights, and because the resulting barge pitch motion exacerbated an already existing problem. In the wind turbine installed on land, the DLC 1.4 simulations ran at rated wind speed generated the largest out-of-plane blade tip deflections and bending moments.

For the land-based wind turbine, DLC 1.3 played a significant roll in driving many of the extreme values of the most relevant output parameters not driven by DLC 1.4. Although we don't present any of the time series, DLC 1.3, with its extreme wind turbulence, was particularly dominant because the resulting wind-inflow contained many drastic jumps or drops in wind speed. And this led to the generation of ultimate loads because the control system could not react fast enough. Jumps in wind speed from below to above rated, or from above to below rated, were particularly bad due to the peak in thrust at rated. Large variations in wind speed near cut-out were also problematic.

The wind turbine mounted on the floating barge was more affected by the waves than the wind, which was why DLC 1.1 in the sea-based analysis, which has the highest effective PSF for loads, dominated the loads results more than DLC 1.3, which has higher levels of wind turbulence. For example, the maximum magnitude of acceleration in the nacelle at the main yaw bearing was 10.1-m/s^2 (just over 1-g) in the floating turbine, as driven by large waves in DLC 1.1, but only 1.4-m/s^2 in the land-based turbine, as driven by extreme wind turbulence in DLC 1.3.

The only loads in the floating system that appeared to be driven more by the wind than waves were the tensions in the mooring lines. The tensions, both at the anchors and the fairleads of the upwind mooring lines in particular, were driven by simulations involving sustained winds at or near rated wind speed. This is because sustained winds at rated generate the highest sustained rotor thrust forces, which pushes the barge far downwind (i.e., a large surge displacement), tugging on the upwind mooring lines. Even at maximum tension however, there was enough slack in the mooring lines to keep them from pulling upwards on the anchors.

In relation to DLCs 1.1, 1.3, and 1.4, DLC 1.5, which considers transient wind-shear events, did not play a significant roll in driving ultimate loads in either the land- or sea-based wind turbine systems.

4. Comparison Between the Land- and Sea-Based Loads

We took the absolute extreme values of each parameter (i.e., the absolute maximum values of the minimums and maximums, from the diagonals of the extreme-events tables) from the sea-based analysis of DLCs 1.1, 1,3, 1.4, and 1.5 and divided them by the corresponding absolute extremes from the land-based analysis. The resulting dimensionless ratios quantify the impact of installing the wind turbine on the floating barge. We present the ratios for many of the parameters in Fig. 10. A ratio of unity (indicated by the dashed horizontal line) would imply that the absolute extreme is unaffected by the dynamic couplings between the turbine and floating barge in the presence of combined wind and wave loading. Ratios greater than unity imply in increase in load or response that may have to be addressed through modifications of the system design in subsequent analysis iterations.

The chart in the upper-left corner of Fig. 10 presents the sea-to-land ratios for the absolute extremes of the generator power, generator torque, generator (high-speed shaft) speed, and rotor (low-speed shaft) speed. The sea-to-land ratio of the generator torque is unity because the variable-speed control system, which is identical in both the land and sea analyses, places a limit on the torque command to avoid excessive overloading of the generator and gearbox. Nevertheless, there are greater generator power excursions in the sea-based system due to the increased excursions in generator speed. This may have to be addressed in the floating wind turbine to avoid generator burn-out. The sea-to-land ratios of the generator and rotor speed are identical because the high- and low-speed shafts are directly coupled through the gearbox. The rotor speed excursions in the floating wind turbine are 60% higher than the excursions seen in the turbine installed on land. These excursions are the result of the oscillatory wind-inflow

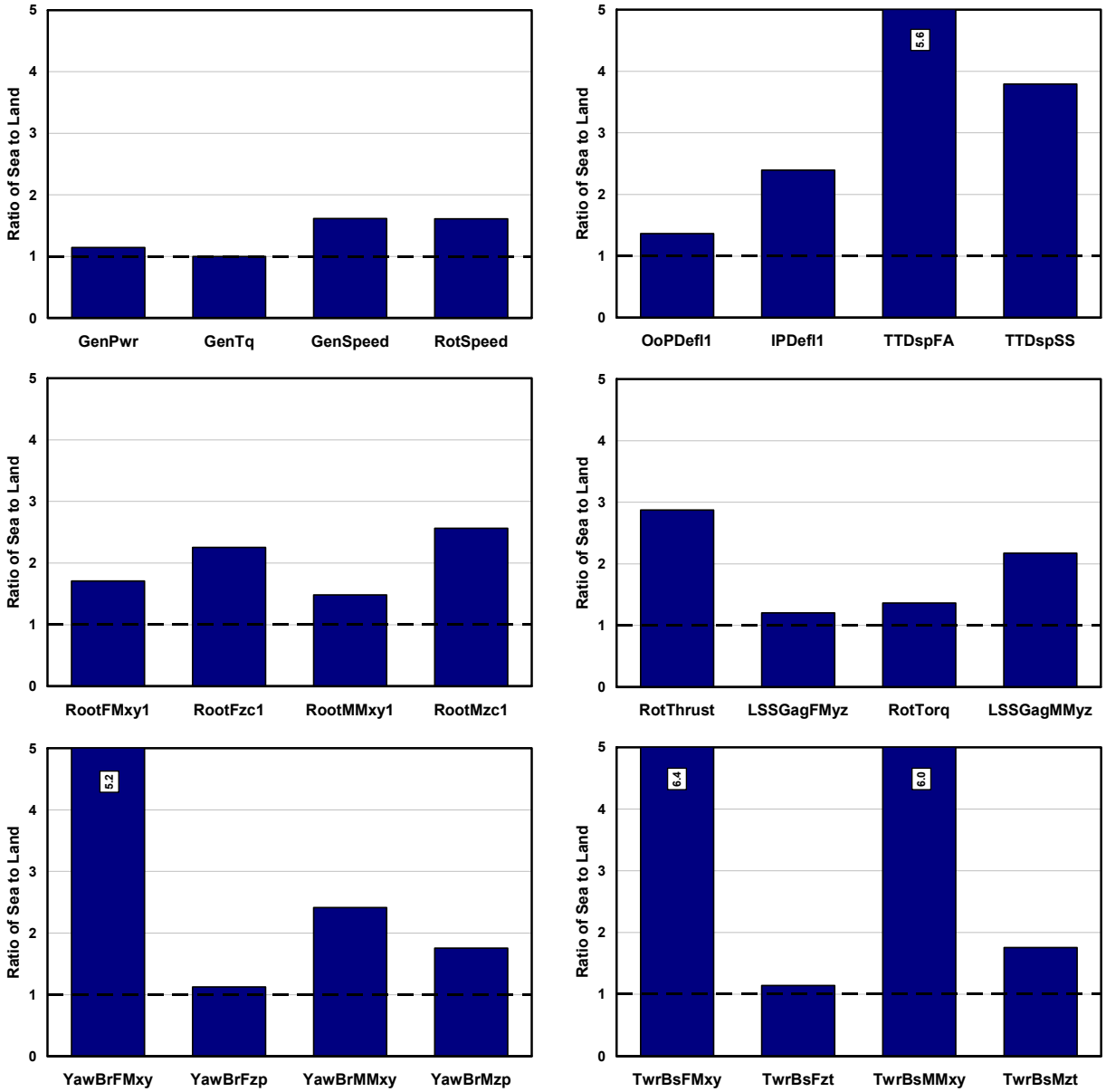

Figure 10. Sea-to-land ratios of absolute extremes from DLCs 1.1, 1.3, 1.4, and 1.5.

relative to the rotor from the pitching motion of the barge, as discussed earlier. They will most assuredly lead to an increase in aeroacoustic emissions from the rotor, which may or may not be important offshore.

The chart in the upper-right corner of Fig. 10 presents the sea-to-land ratios for the absolute extremes of the out-of-plane and in-plane tip deflections of blade 1 and the fore-aft and side-to-side displacements of the tower-top. The sea-to-land ratio for the tower-top fore-aft displacement exceeds the upper bound of 5 placed on the ordinate, which is why its value of 5.6 is listed. This ratio is much larger than the sea-to-land ratio of the out-of-plane blade tip deflection due again to the inverted pendulum effect discussed earlier. The larger excursions of in-plane blade tip deflection in the sea-based system are the result of faster rotor rotational accelerations, corresponding with the elevated excursions in rotor speed. The tower side-to-side displacements are larger in the floating wind turbine due to the presence of larger yaw errors between the nominal wind direction and the rotor axis. These, in turn, come from the yaw motion of the barge, which is excited by a gyroscopic yaw moment that results from the spinning inertia of the rotor in combination with the pitching motion of the barge. Larger yaw motions are permissible because of the yaw compliance of the mooring system.

The remaining charts in Fig. 10, from the middle-left corner to the lower-right corner, present the sea-to-land ratios for the absolute extremes of the forces and moments in the root of blade 1, in the low-speed shaft at the main

bearing, in the yaw bearing, and in the tower base, respectively. In the parameter names, "FMxy" refers to the magnitude of the internal shear force in the transverse x- and y-plane of the various coordinate systems. These were found by taking the vector sum of the shear forces along the x- and y-axes. Likewise, "MMxy" refers to the magnitude of the internal bending moment in the transverse x- and y-plane of the various coordinate systems that was found by taking the vector sum of the bending moments about the x- and y-axes. We computed the maximum values of the vector sums as opposed to the more-conservative calculation of the vector sums of the maximum values. The remaining parameters refer to the axial forces along, and the torsion moments about, the primary axis of the members.

The sea-to-land ratios of the internal shear force and bending moment magnitudes, in general, increase as one follows the load path from the blade tip, through the drivetrain and nacelle, to the tower base. This increase in relative loading between the sea- and land-based systems results again from the inverted pendulum effect in the floating wind turbine. That is, there is more effect of loading from inertia farther down the load path. The axial forces in the blades are increased in the floating wind turbine relative to the onshore turbine due to the centripetal effect from elevated excursions in rotor speed. The axial forces at the yaw bearing and tower base are larger in the floating system than the onshore system due to the heave motion of the barge as it follows the up and down elevation of the waves. The sea-to-land ratio of the rotor thrust, "RotThrust," is large because it is computed not as the applied aerodynamic thrust, but as the internal force within the low-speed shaft, which by d'Alembert's principle,[41] is the difference between the applied thrust and the fore-aft rotor inertia acceleration or deceleration. The inertia effect itself is large again because of the barge pitch motion. To withstand the increased loading, the tower will certainly, and the blades and drivetrain as well may, have to be strengthened for the wind turbine mounted on the floating barge.

Of course, all of the results presented so far were derived from the environmental conditions at our reference site. To repeat what we stated in section III.C, our reference site was chosen for its fairly extreme wind and wave conditions, with the implication that if the results of the loads analysis are favorable, then the floating wind turbine system under consideration will be applicable at almost any site worldwide. The loads analysis results indicate, however, that without modification of the design, there is potential for loads in the floating wind turbine that are much larger (up to 6.4 times as large at the tower base as indicated in Fig. 10) than what would be seen in an equivalent onshore wind turbine. Because of this, it is beneficial to examine whether or not the existing concept, without modification, may be better suited at a less severe site.

We studied the effect of the choice in reference site by rerunning the sea-based loads analysis with varying environmental conditions. Instead of choosing different locations to re-obtain metocean data, we took a simpler approach and obtained varying environmental conditions by modifying the existing data from our chosen reference site. We chose to adjust only the data of significant wave height because the size of the waves was the key parameter that led to the excessive pitching of the barge and subsequent loading of the floating wind turbine. We did not modify the wind speed data because we wanted to maintain a fair comparison to the results from the land-based wind turbine, which is unaffected by wave conditions. We did not modify the wave period data because the range of wave periods considered are typical of sites worldwide, and because we did not want to adversely affect the wave steepness. (The wave steepness is related to the wave height and wavelength, the later of which is dictated by the wave frequency or period.) We adjusted the data of significant wave height by scaling down the magnitude of each data sample provided by the Waveclimate.com service, which corresponds with scaling consistently across all other conditions. We chose wave height scaling factors of 75%, 50%, 25%, and 0%. For example, with a wave height scaling factor of 50%, the expected value of the significant wave height would increase with the mean hub-height wind speed that it is conditioned on, from about 0.8 m instead of 1.6 m at cut-in, V_{in} = 3 m/s, to about 3.0 m instead of 5.9 at cut-out, V_{out} = 25 m/s (the original data is plotted in Fig. 6). A wave height scaling factor of 0% represents still water with no incident waves (but outgoing waves can still be generated by wave radiation).

We reran the sea-based loads analysis with the reference site data adjusted by each wave height scaling factor. Figure 11 presents the sea-to-land ratios for the absolute extremes from the rerun loads analysis of DLCs 1.1, 1.3, 1.4, and 1.5. The leftmost ratios of each parameter, labeled "100% - Original," correspond to the ratios presented in Fig. 10 resulting from the original reference site data. The remaining ratios of each parameter correspond with decreasing severity in the wave conditions, from left to right. For most parameters, the sea-to-land ratios decline rapidly at first, then drop off more slowly with decreasing severity in the wave conditions. So interestingly, the response is nonlinear even though the hydrodynamic model is based on linear radiation and diffraction theory. This implies that other nonlinear features of the model; such as aerodynamic loading, turbine dynamics, and control actions; are affecting the response. Moreover, even in still water, the wind turbine mounted on the barge experiences higher loading than the turbine that is installed on land. In fact, the absolute extreme magnitude of the internal bending moment at the base of the tower is still 60% higher in the floating wind turbine in still water than in

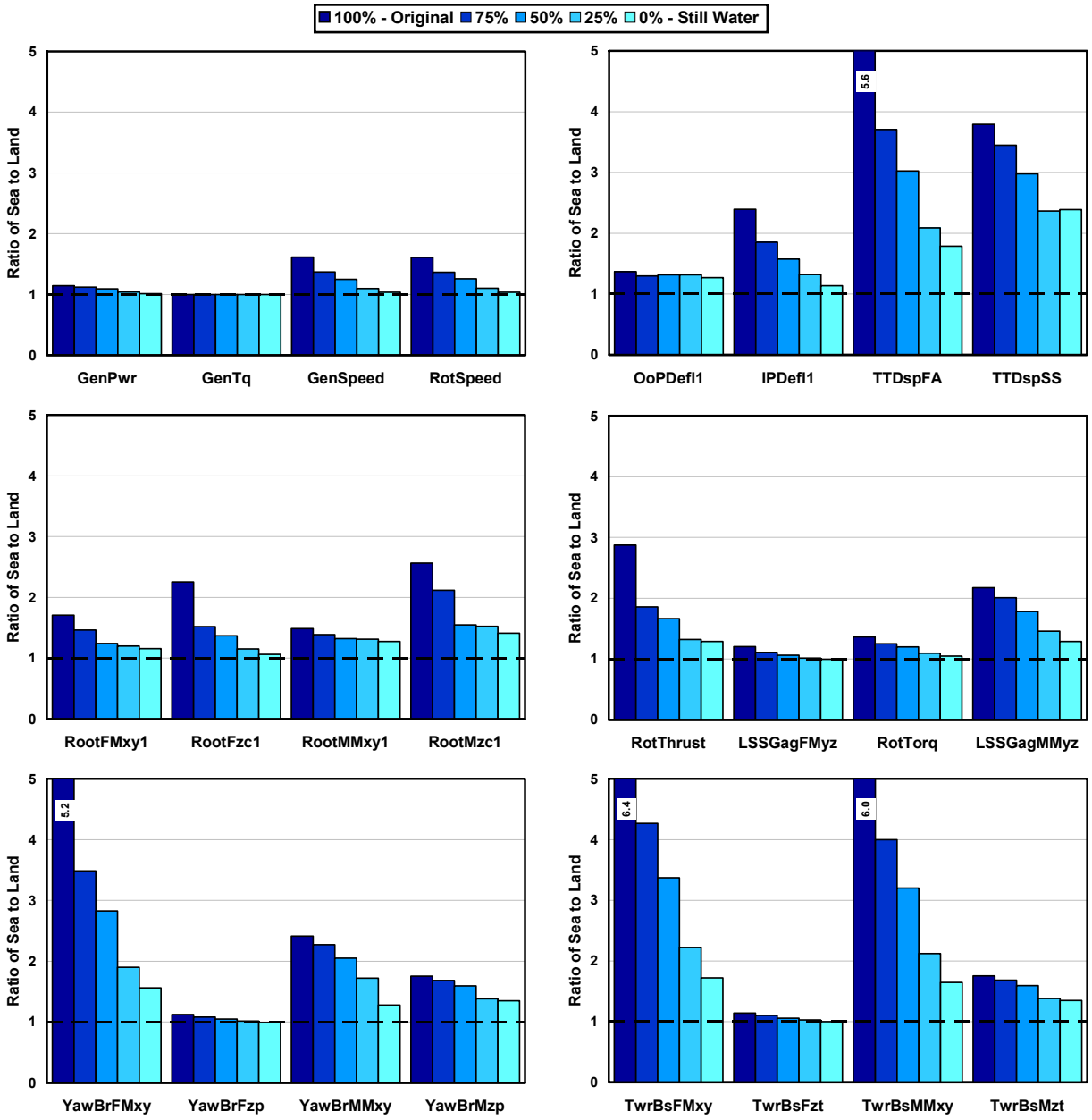

Figure 11. Sea-to-land ratios of absolute extremes for variations in significant wave height.

the turbine on land. This implies that the barge pitches because of turbulence in the wind-inflow, as well as wave excitation. Nevertheless, the results show that the potential loads in the floating wind turbine will be considerably less at a sheltered site than at a site in the open ocean.

5. Conclusions Regarding the Systems Responses in Normal Operation

In summary of the results presented in this section, the pitching motion of the barge brings about load excursions in the supported wind turbine in excess of what is experienced by the turbine that is installed on land. The load excursions are worse in the tower than in the blades due to the increased effect of inertia from the barge pitch motion. To arrive at a technically feasible concept, modifications to the design will be required, except possibly at the most sheltered of sites. This is not surprising, however, because we made no attempt to minimize the floating platform motions in our present analysis, which was the first step of the design iteration process outlined in the beginning of section IV. Two forms of design modifications are possible. First, the turbine, especially the tower, could be strengthened so as to enable it to withstand the increased loading. However, this avenue may not be cost effective even though the wind turbine in an offshore floating system is a smaller fraction of the total installed cost

than on land. Second, design alterations may be able to improve the response of the floating system to diminish the increases in loading.

One possible avenue to improving the response of the floating system is to add design features that will increase damping to stabilize the barge pitch motion. In ITI Energy's original concept, not only is the barge designed to support the NREL offshore 5-MW baseline wind turbine, but it is also a platform for an OWC wave power device, which we unfortunately could not model with our present simulation tool as described in section III.B. But if positioned suitably and controlled properly, the OWC may be able to introduce damping of the barge pitch motion while extracting wave energy. This concept is currently being researched through analytical modeling and wave tank testing at the Department of Naval Architecture and Marine Engineering at the Universities of Glasgow and Strathclyde.[10] Other actuator opportunities include gyro actuators, used commonly for system stabilization in aerospace and spacecraft applications, or hydrodynamic thrusters, used commonly for station keeping in naval architecture.

It may also be possible to develop a wind turbine control system; which relies on the conventional wind turbine actuation of blade pitch, generator torque, and nacelle yaw; to dampen the barge pitch motion. We've examined possible control methodologies in a study performed in parallel to our loads analysis, but the results are beyond the scope of this paper.

Beyond active control, a simpler solution for improving the barge pitch damping may be to introduce passive damping devices into the underlying design. Tuned mass dampers (TMDs) are frequently employed in skyscrapers to dampen wind-induced vibrations. Similarly, a TMD could be placed at the top of the wind turbine tower; when tuned at the natural period of the rigid-body turbine plus barge pitch mode, such a system could dampen pitching (and rolling) motion dramatically. It may also be possible to dampen the barge rotational motions with the equivalent of passive anti-roll stabilizers installed within or on top of the barge. (Anti-roll stabilizers, which are commonly installed on ships, act like TMDs, but are made of water-filled U-tube tanks.[19]) The platform's hydrodynamic radiation damping and viscous drag could also be increased through the incorporation of damping orifices in the planform of the barge or horizontal damping plates and/or bilge keels positioned below the free surface.

Instead of trying to improve the barge pitch damping, it may be better to add DOFs in or between the floating platform and the wind turbine to eliminate the direct coupling between the platform motions and turbine motions. For example, articulated joints may be installed in the floating platform, as in the Versabuoy offshore system,[‡‡‡] or between the wind turbine's tower and nacelle, as in the Wind Eagle turbine.[42]

Finally, the easiest solution may be to modify the geometry of the floating platform and/or layout of the mooring system so as to reduce the barge's natural pitch motion, and consequently, to minimize the impact to the supported wind turbine. Possibilities include streamlining the shape of the barge to allow surface waves to more easily pass by (i.e., more like in a Spar-buoy), shifting the center of gravity closer to the center of buoyancy through ballast (i.e., like in a Spar-buoy), or introducing tauter mooring lines (i.e., like in a TLP).

B. Other Load Cases

As mentioned in the introduction to section V, we identified problems with both the land- and sea-based system configurations when we processed the loads analysis results for DLCs 1.6a, 2.x, 6.x, and 7.1a, which are concerned with the wind turbine when it is experiencing a fault, when it is idling, and/or when it is being excited by 1- and 50-yr wind and wave conditions. We describe these problems in more detail here. But because the loads resulting from the problems were unreasonable, we don't quantify them in this paper. We also discuss potential design modifications that may be used to correct the problems.

In relation to DLCs 1.6a, 2.1, 6.x, and 7.1a, DLC 2.3, which considers an extreme operating wind gust concurrent with a loss of load, and which we did not include in the results of section V.A because of the way we split the results into meaningful groups, did not cause problems in either the land- or sea-based wind turbine systems. Consequently, we do not discuss any of the results from DLC 2.3 in our subsequent presentation.

1. Tower Side-to-Side Instability of Land-Based Wind Turbine

The first problem we discovered was a side-to-side instability in the tower of the wind turbine that is installed on land. We identified this instability when analyzing the loads predicted by land-based DLC 6.2a. The instability occurs when the turbine is idling with all blades fully-feathered to the maximum pitch setting of 90º, but only when the rotor is positioned at certain azimuth angles and is misaligned with the mean wind direction by about plus or minus 20º to 40º. (DLC 6.2a considers the full range of yaw misalignments because of an assumed inability of the yaw controller to align the rotor with the wind during a situation in which electrical power is unavailable while the

[‡‡‡] Website: http://www.vbuoy.com/index.html.

grid is lost.) DLC 6.2a required us to analyze this situation with extreme 50-yr wind conditions, V_{50} = 50 m/s, but after more study, we discovered that the instability is predicted by our simulation tools at much lower wind speeds, as low as a mean hub-height wind speed of 25 m/s. The instability is more severe, however, at the higher wind speeds. The instability leads to excessive limit cycle oscillations in the tower top side-to-side displacement and the tower base side-to-side (roll) bending moment. The oscillations occur at about 0.32 Hz, which corresponds with the natural frequency of the first side-to-side bending mode of the tower.

In the sea-based simulations of DLC 6.2a, it is difficult to distinguish an instability from the excessive barge motions generated by the extreme 50-yr wave conditions (described as the third problem below). So we reanalyzed the floating wind turbine with all of the specifications of DLC 6.2a except the 50-yr wave conditions, which we replaced with still water. In this situation, the instability is nonexistent. So, fascinatingly, the barge compliance actually helps to eradicate the side-to-side instability in the land-based tower, at least when there are no incident surface waves present. That is, the tower is prevented from going unstable due to the compliance of the barge in still water.

The instability in the land-based turbine almost certainly exists because the amount of structural damping in the first side-to-side bending mode of the tower is exceeded by the amount of energy the rotor absorbs within the critical range of azimuth and yaw error angles, probably because of the range of wind-inflow angles-of-attack on the blades during those conditions. However, it is difficult to determine what causes what because of the classic chicken and egg problem. That is, which comes first; the oscillation in angles of attack or the instability? Also, it is difficult to determine if the predicted instability is physical or an artifact of our analysis. As described in section IV.A, we ran this DLC without AeroDyn's induction or dynamic stall models enabled because they are not applicable in this idling case, particularly at very high post-stall angles-of-attack. It may be worthwhile to examine the time histories of angles-of-attack to determine if the simple table-lookup aerodynamic methods that we used are adequate in this situation and to determine if other aerodynamic theories are more appropriate and would predict different behavior. But we did not consider this action necessary at this time.

Nevertheless, the information we do know about the tower side-to-side instability of the land-based wind turbine suggests two possible remedies that may be pursued if the problem is real instead of virtual. First, it may be possible to modify the shape of the airfoils in the blades to reduce the amount of energy absorption at the problematic angles-of-attack. Second, it may be possible to apply a fail-safe brake to park the rotor in extreme winds and to keep it away from the critical azimuth positions. The downside to this second solution is that it may cause excessive wear on the brake and be a source of routine maintenance. We show that this solution does work, however, in the time history presented in Fig. 12. This figure shows the results of two separate FAST simulations. The first simulation considered the onshore wind turbine idling with all blades fully-feathered in steady, uniform 50-m/s winds, and a yaw error of 30º. The second simulation used the same set of conditions, but at 150 s into the simulation, we applied a high-speed shaft brake. Before the brake is engaged, the responses predicted by the two simulations are identical. After the brake is engaged, the amplitude of the limit cycle oscillation in the tower top side-to-side displacement is reduced significantly. (The cycles are very close together and difficult to discern because the frequency of about 0.32 Hz is small for the range of simulation times considered on the abscissa.)

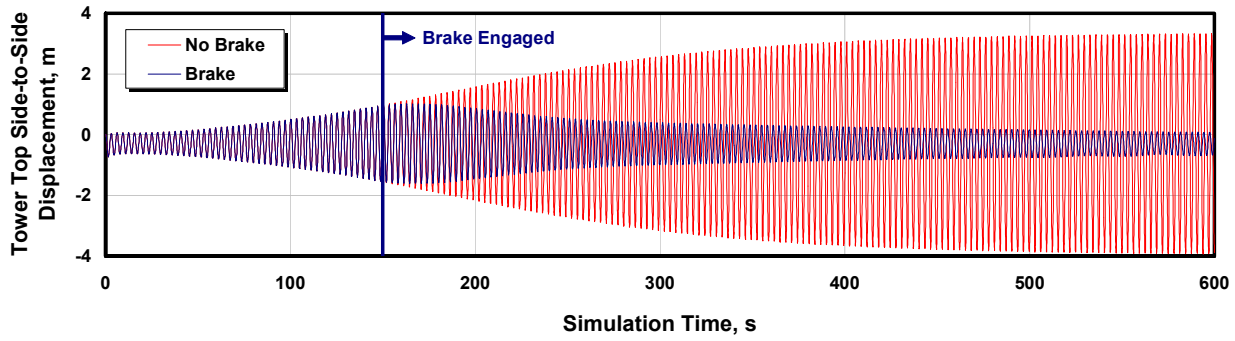

Figure 12. Time history of the tower side-to-side instability with and without application of a brake.

2. Platform Yaw Instability of Sea-Based Wind Turbine

The second problem we discovered was a yaw instability in the barge of the floating wind turbine. The instability occurs when the rotor is idling with a fault, where one blade (the faulted blade) is seized at the minimum pitch set-point of 0º, while the other two blades are fully-feathered to the maximum pitch setting of 90º. We identified this instability when analyzing the loads predicted by sea-based DLCs 2.1 and 7.1a. In DLC 2.1, which

considers normal wind and wave conditions, the instability occurs after the turbine is shut down by the protection system due to its detection of the blade pitch fault. The instability is more severe in DLC 7.1a, which required us to analyze this fault condition under extreme 1-yr wind and wave conditions, with misalignments in the mean wind and wave directions of plus or minus 8º and plus or minus 30º, respectively. After more study, however, we discovered that the instability is predicted by our simulation tools regardless of the yaw misalignment and also in still water. The instability is caused by a coupling of the barge yaw motion with the azimuthal motion of the seized blade, and leads to excessive limit cycle oscillations in the barge yaw displacement. This, in turn, may cause a knotting of the mooring lines (though our simulation tool cannot model line-to-line interference) and/or excessive loading of the wind turbine from the ensuing dynamics. The oscillations occur at about 0.02 Hz, which corresponds with the natural frequency of the rigid-body turbine plus barge yaw mode.

The idling plus fault condition does not cause a problem in the land-based wind turbine because it has very little yaw compliance. This condition may cause problems, however, that are more pronounced in floating Spar-buoy or TLP concepts than in our floating barge because the former concepts are likely to be more compliant in yaw because of smaller moment arms available to resist yaw forces. In the floating barge, the yaw instability may also be less severe than our simulation tools predict because our model considers hydrodynamic damping in yaw only from wave radiation (i.e., potential flow), which is negligible at the yaw mode natural frequency. In actuality, hydrodynamic viscous damping in yaw may be more dominant. Hydrodynamic viscous damping in yaw comes from vortex shedding off the corners of the barge and skin friction, neither of which are accounted for in our model. It may be worthwhile trying to quantify the viscous drag contributions through wave tank tests for the vortex shedding drag and/or ship resistance formulas for the skin friction drag to see if they provide enough damping to eliminate the yaw instability. But as in our investigation of the tower side-to-side instability, we did not consider this action necessary at this time.

As in the tower side-to-side instability, there are several pathways that may be pursued to eliminate the yaw instability of the barge if the problem is real instead of virtual. Possibilities include supplementing the existing yaw damping by installing damping plates below the free surface, increasing the yaw stiffness by adding a so-called "crowfoot" at the connection between the mooring line and the barge, applying a fail-safe shaft brake to park the rotor when shut down, or reducing the pitch angle of the fully-feathered blades to generate a low, but persistent, aerodynamic torque that will produce a slow roll of the rotor while idling. The later two solutions would prevent the seized blade from coupling with the platform yaw motion. We tested the brake approach again with FAST simulations and present the results in Fig. 13. The first simulation considered the floating wind turbine idling with one blade flat into the wind (faulted) and with steady uniform 40-m/s winds and no incident surface waves (still water). The second simulation used the same set of conditions, but at 100 s into the simulation, we applied a high-speed shaft brake. Before the brake is engaged, the responses predicted by the two simulations are identical. After the brake is engaged, the limit cycle oscillation in the barge yaw displacement is eliminated.

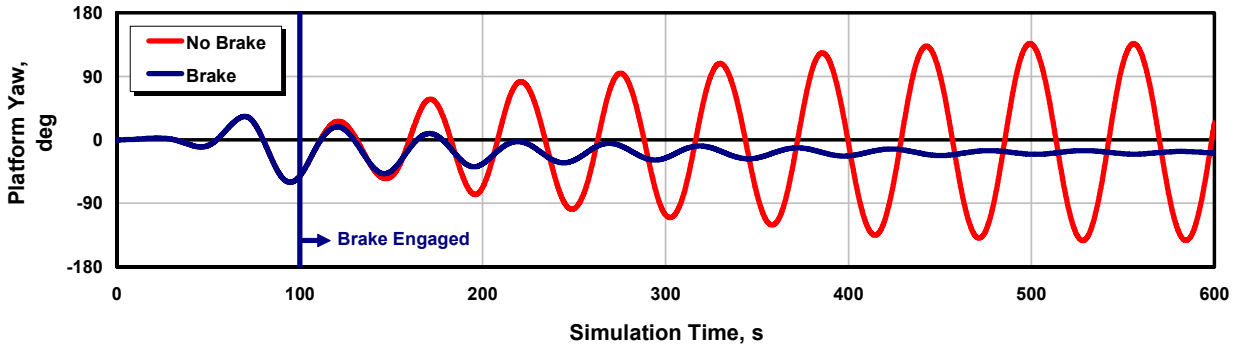

Figure 13. Time history of the barge yaw instability with and without application of a brake.

3. Susceptibility of Barge to Excessive Motions in Extreme Waves

The final problem we discovered through our loads analysis was that the floating barge is susceptible to excessive motions when the incident waves are large and/or steep, such as during extreme 1- or 50-yr wave conditions. This is especially true with the harsh conditions that occur at our chosen reference site. The problems exist whether the wind turbine is idling, as in DLCs 6.x and 7.1a, or producing power, as in DLC 1.6a. The response is worse, however, in the idling turbine because the operating turbine introduces more aerodynamic damping. The response is also worse in the 50-yr wave conditions than in the 1-yr conditions. The problems in

DLCs 1.6a or 6.x are not related to a system instability because the problems go away in the simulations were the extreme wave conditions are exchanged with still water.

The motions usually occur in a series of stages. First, the barge begins to pitch back and forth as it moves with the surface waves. The large pitching motion leads to excessive deflections in the blades and tower of the wind turbine. When the blades deflect asymmetrically, due to variations in the rotor azimuth angle, turbulence in the wind, or misalignment of the waves from barge's planes of symmetry, the barge gets excited in other modes of motion, such as roll and yaw. The overall result is excessive deflections and loading throughout the entire system, from the blades to the moorings. The problem is so bad that even though the blade tips of the undeflected or undisplaced floating turbine are positioned 30 m above the still water level, the system gets jostled so severely that the blade tips pass below the free surface in many of the DLC simulations involving 1- and 50-yr wave conditions.

All of the simulations that exhibit this problem consist of waves and responses that most assuredly violate linear radiation and diffraction theory. And our simulation tool is invalid in these situations. It is unclear, however, whether the "real" responses would fair better or worse. This is simply a fundamental limitation with our analysis, if not with most other computational capabilities available in the offshore industry today. To get around these limitations, wave tank testing of a scaled model under equivalent conditions are required. This work has already been initiated at the Department of Naval Architecture and Marine Engineering at the Universities of Glasgow and Strathclyde.[10]

More likely than not, modifications to the system design will be required to eliminate the vulnerability of the barge to extreme waves, unless the barge is only installed at sheltered sites. Except those that involve active wind turbine control, which are not applicable in an idling turbine, or active control of other actuators, which can't always be relied on during extreme events, the design modifications listed at the end of section V.A will help to solve this problem. We plan to examine many of these design modifications in follow-on projects, the results of which we will present in future papers.

VI. Conclusion

Limitations of previous time and frequency domain studies on floating offshore wind turbines motivated our development of simulation capability for modeling the fully coupled aero-hydro-servo-elastic response of such systems. We used this simulation capability to perform a preliminary, but integrated, loads analysis for the NREL offshore 5-MW baseline wind turbine mounted both on land and offshore on the floating ITI Energy barge, which has slack, catenary moorings. We based our analysis on the ultimate load cases and procedures dictated by the on- and offshore IEC wind turbine design standards and the severe environmental conditions at a reference site in the northern North Sea. By comparing the responses of the land- and sea-based systems, we were able to quantify the impact brought about by the dynamic couplings between the turbine and floating barge in the presence of combined wind and wave loading.

We characterized the dynamic responses by showing that the mean values of the loads and deflections in the floating turbine are very similar to, but the excursions of the loads and deflections exceed, those that exist on land. We showed that the increased load excursions in the floating system were produced by the pitching motion of the barge, and so were higher in the tower than in the blades because of the increased effect of inertia. We discussed how the barge concept was susceptible to excessive pitching during extreme wave conditions, but showed how the load excursions reduce with decreasing severity in the waves. Relative to the fixed land-based support, we found that the added compliance in the barge led to an instability of the floating system in yaw when the wind turbine was idling with a faulted blade. We discussed how the compliance of the floating barge did, however, mitigate a tower side-to-side instability discovered in the land-based turbine. We suggested design modifications and active and passive control features that could reduce the barge motions, improve the turbine response, and eliminate the instabilities. If we can solve the design challenges in an economically feasible way, we will open up the possibility for using offshore floating wind turbines to power much of the world with an indigenous, nonpolluting, and inexhaustible energy source.

Future Work

We plan to develop advanced control methodologies and make design modifications to the wind turbine and floating barge concept to reduce the barge motions, improve the turbine response, and eliminate the instabilities. We will then rerun the loads analysis to assess the concept's technical and economic feasibility. When we do this, we would like to expand the set of load cases considered to quantify the impact of the platform motions on the fatigue life of the supported wind turbine. We also plan to perform loads analyses on the other promising offshore

floating support platform configurations to determine which one shows the most promise for harnessing the vast worldwide deepwater wind resource.

Additional code enhancements to improve the simulation of floating offshore wind turbines are possible. For example, we would like to add capabilities that will allow us to test various mechanisms for stabilizing the barge pitch motion, such as TMDs, OWCs, or other active and passive control devices. We would like to introduce second-order effects into our hydrodynamics module, including the effects of intermittent wetting and mean-drift, slow-drift, and sum-frequency excitation, which are necessary for accurate modeling of TLP designs and in the analysis of general support platforms subject to large and/or steep waves. We would also like to replace our quasi-static mooring system module with a fully coupled module that can handle the dynamics of the lines. Though not specific to the modeling of offshore wind turbines, we also plan to add a torsion DOF to the modal representation of the tower in FAST, and to extend the modal representation of the blades to include mass and elastic offsets, torsion DOFs, and coupled mode-shape properties.

Acknowledgments

We would like to thank everyone who helped with this work, including Ian Edwards of ITI Energy for sponsoring the loads analysis project and Dr. Nigel Barltrop and Willem Vijfhuizen of the Universities of Glasgow and Strathclyde for designing the barge and mooring system concept. We also thank Walt Musial and Sandy Butterfield of NREL for leading the offshore wind energy program there; Jason Jonkman's Ph.D. committee members at the University of Colorado at Boulder, the University of Wyoming, NREL, and MIT for evaluating the project; and Bruce Green of NREL, for editing this paper to make it much more readable.

This work was performed at NREL in support of the U.S. Department of Energy under contract number DE-AC36-99-GO10337 and in support of a Cooperative Research and Development Agreement with ITI Energy, number CRD-06-178.

References

[1]Musial, W.; Butterfield, S.; and Ram, B., "Energy From Offshore Wind," *2006 Offshore Technology Conference, 1–4 May 2006, Houston, TX* [CD-ROM], Richardson, TX: Offshore Technology Conference, May 2006, OTC 18355, NREL/CP-500-39450.

[2]Musial, W.; Butterfield, S.; and Boone, A., "Feasibility of Floating Platform Systems for Wind Turbines," *A Collection of the 2004 ASME Wind Energy Symposium Technical Papers Presented at the 42nd AIAA Aerospace Sciences Meeting and Exhibit, 5–7 January 2004, Reno Nevada, USA*, New York: American Institute of Aeronautics and Astronautics, Inc. (AIAA) and American Society of Mechanical Engineers (ASME), January 2004, pp. 476–486, NREL/CP-500-36504.

[3]Watson, G., et al, "A Framework for Offshore Wind Energy Development in the United States," *Massachusetts Technology Collaborative (MTC)* [online publication], URL: http://www.mtpc.org/offshore/final_09_20.pdf, [cited 17 November 2005].

[4]Musial, W. and Butterfield, S., "Future for Offshore Wind Energy in the United States," *EnergyOcean Proceedings, June 2004, Palm Beach Florida, USA*, NREL/CP-500-36313.

[5]Butterfield, S.; Musial, W.; Jonkman, J.; Sclavounos, P.; and Wayman, L., "Engineering Challenges for Floating Offshore Wind Turbines," *Copenhagen Offshore Wind 2005 Conference and Expedition Proceedings, 26–28 October 2005, Copenhagen, Denmark* [CD-ROM], Copenhagen, Denmark: Danish Wind Energy Association, October 2005.

[6]Bulder, B. H., et al, "Study to Feasibility of and Boundary Conditions for Floating Offshore Wind Turbines," Novem 2002-CMC-R43, ECN, MARIN, Lagerway the Windmaster, TNO, TUD, MSC, December 2002.

[7]Lee, K. H., "Responses of Floating Wind Turbines to Wind and Wave Excitation," M.S. Dissertation, Department of Ocean Engineering, Massachusetts Institute of Technology, Cambridge, MA, USA, January 2005.

[8]Wayman, E. N.; Sclavounos, P. D.; Butterfield, S.; Jonkman, J.; and Musial, W., "Coupled Dynamic Modeling of Floating Wind Turbine Systems," *2006 Offshore Technology Conference, 1–4 May 2006, Houston, TX* [CD-ROM], Richardson, TX: Offshore Technology Conference, May 2006, OTC 18287, NREL/CP-500-39481.

[9]Wayman, E., "Coupled Dynamics and Economic Analysis of Floating Wind Turbine Systems," M.S. Dissertation, Department of Mechanical Engineering, Massachusetts Institute of Technology, Cambridge, MA, USA, June 2006.

[10]Vijfhuizen, W. J. M. J, "Design of a Wind and Wave Power Barge," M.S. Dissertation, Department of Naval Architecture and Mechanical Engineering, Universities of Glasgow and Strathclyde, Glasgow, Scotland, September 2006.

[11]Henderson, A. R. and Patel, M. H., "On the Modelling of a Floating Offshore Wind Turbine," *Wind Energy*, Vol. 6, No. 1, February 2003, pp. 53–86.

[12]Fulton, G. R., Malcolm, D. J., and Moroz, E., "Design of a Semi-Submersible Platform for a 5MW Wind Turbine," *44th AIAA Aerospace Sciences Meeting and Exhibit, 9–12 January 2006, Reno, NV, AIAA Meeting Papers on Disc* [CD-ROM], Reston, VA: American Institute of Aeronautics and Astronautics, January 2006, AIAA-2006-997.

[13]Withee, J. E., "Fully Coupled Dynamic Analysis of a Floating Wind Turbine System," Ph.D. Dissertation, Department of Ocean Engineering, Massachusetts Institute of Technology, Cambridge, MA, USA, 2004.

[14]Nielsen, F. G., Hanson, T. D., and Skaare, B., "Integrated Dynamic Analysis of Floating Offshore Wind Turbines," *Proceedings of OMAE2006 25th International Conference on Offshore Mechanics and Arctic Engineering, 4–9 June 2006, Hamburg, Germany* [CD-ROM], Houston, TX: The American Society of Mechanical Engineers (ASME International) Ocean, Offshore and Arctic Engineering (OOAE) Division, June 2006, OMAE2006-92291.

[15]Skaare, B., Hanson, T. D., and Nielsen, F. G., "Importance of Control Strategies on Fatigue Life of Floating Wind Turbines," *Proceedings of OMAE2007 26th International Conference on Offshore Mechanics and Arctic Engineering, 10–15 June 2007, San Diego, CA* [CD-ROM], Houston, TX: The American Society of Mechanical Engineers (ASME International) Ocean, Offshore and Arctic Engineering (OOAE) Division, June 2007, OMAE2007-29277.

[16]Zambrano, T., MacCready, T., Kiceniuk, T., Jr., Roddier, D. G., and Cermelli, C. A., "Dynamic Modeling of Deepwater Offshore Wind Turbine Structures in Gulf of Mexico Storm Conditions," *Proceedings of OMAE2006 25th International Conference on Offshore Mechanics and Arctic Engineering, 4–9 June 2006, Hamburg, Germany* [CD-ROM], Houston, TX: The American Society of Mechanical Engineers (ASME International) Ocean, Offshore and Arctic Engineering (OOAE) Division, June 2006, OMAE2006-92029.

[17]Zambrano, T., MacCready, T., Roddier, D. G., and Cermelli, C. A., "Design and Installation of a Tension Moored Wind Turbine," *Proceedings of OMAE2007 26th International Conference on Offshore Mechanics and Arctic Engineering, 10–15 June 2007, San Diego, CA* [CD-ROM], Houston, TX: The American Society of Mechanical Engineers (ASME International) Ocean, Offshore and Arctic Engineering (OOAE) Division, June 2007, OMAE2007-29587.

[18]Newman, J. N., *Marine Hydrodynamics*, The MIT Press, Cambridge, MA, USA, 1997.

[19]Faltinsen, O. M., *Sea Loads on Ships and Offshore Structures*, Cambridge University Press, Cambridge, UK, 1990.

[20]Cummins, W. E., "The Impulse Response Function and Ship Motions," *Schiffstechnik*, Vol. 9, October 1962, pp. 101–109.

[21]Ogilvie, T. F. "Recent Progress toward the Understanding and Prediction of Ship Motions," *Fifth Symposium on Naval Hydrodynamics*, September, 1964, pp. 3–128.

[22]IEC 61400–1 Ed. 3, *Wind Turbines – Part 1: Design Requirements*, International Electrotechnical Commission (IEC), 2005.

[23]IEC 61400–3, *Wind Turbines – Part 3: Design Requirements for Offshore Wind Turbines*, International Electrotechnical Commission (IEC), 2006 (to be published).

[24]Jonkman, J. M. and Sclavounos, P. D., "Development of Fully Coupled Aeroelastic and Hydrodynamic Models for Offshore Wind Turbines," *44th AIAA Aerospace Sciences Meeting and Exhibit, 9–12 January 2006, Reno, NV*, *AIAA Meeting Papers on Disc* [CD-ROM], Reston, VA: American Institute of Aeronautics and Astronautics, January 2006, AIAA-2006-995, NREL/CP-500-39066, Golden, CO: National Renewable Energy Laboratory.

[25]Jonkman, J. M. and Buhl, M. L., Jr., "Development and Verification of a Fully Coupled Simulator for Offshore Wind Turbines," *45th AIAA Aerospace Sciences Meeting and Exhibit, 8–11 January 2007, Reno, NV*, *AIAA Meeting Papers on Disc* [CD-ROM], Reston, VA: American Institute of Aeronautics and Astronautics, January 2007, AIAA-2007-212, NREL/CP-500-40979, Golden, CO: National Renewable Energy Laboratory.

[26]Jonkman, J. M. and Buhl, M. L., Jr., "FAST User's Guide," NREL/EL-500-29798, Golden, CO: National Renewable Energy Laboratory, October 2004.

[27]Laino, D. J. and Hansen, A. C., "User's Guide to the Wind Turbine Dynamics Aerodynamics Computer Software AeroDyn," Salt Lake City, UT: Windward Engineering LLC, Prepared for the National Renewable Energy Laboratory under Subcontract No. TCX-9-29209-01, December 2002.

[28]Moriarty, P. J. and Hansen, A. C., "AeroDyn Theory Manual," NREL/EL-500-36881, Golden, CO: National Renewable Energy Laboratory, December 2005.

[29]Laino, D. J. and Hansen, A. C., "User's Guide to the Computer Software Routines AeroDyn Interface for ADAMS®," Salt Lake City, UT: Windward Engineering LLC, Prepared for the National Renewable Energy Laboratory under Subcontract No. TCX-9-29209-01, September 2001.

[30]Elliott, A. S., "Analyzing Rotor Dynamics with a General-Purpose Code," *Mechanical Engineering*, Vol. 112, No. 12, December 1990, pp. 21–25.

[31]Lee, C. H. and Newman, J. N., "WAMIT® User Manual, Versions 6.3, 6.3PC, 6.3S, 6.3S-PC," WAMIT, Inc., Chestnut Hill, MA, USA, 2006.

[32]Jonkman, B. J. and Buhl, M. L., Jr., "TurbSim User's Guide," NREL/EL-500-41136, Golden, CO: National Renewable Energy Laboratory, March 2007.

[33]Laino, D. J, "IECWind: A Program to Create IEC Wind Data Files," *NWTC Design Codes* [online database], URL: http://wind.nrel.gov/designcodes/preprocessors/iecwind/ [cited 22 July 2005].

[34]Saigal, R. K.; Dolan, D.; Der Kiureghian, A; Camp, T.; and Smith, C. E., "Comparison of Design Guidelines for Offshore Wind Energy Systems," *2007 Offshore Technology Conference, April 30 – May 3, 2007, Houston, TX* [CD-ROM], Richardson, TX: Offshore Technology Conference, May 2007, OTC 18984.

[35]Agarwal, P. and Manuel, L., "Simulation of Offshore Wind Turbine Response for Extreme Limit States," *Proceedings of OMAE2007 26th International Conference on Offshore Mechanics and Arctic Engineering, 10–15 June 2007, San Diego, CA* [CD-ROM], Houston, TX: The American Society of Mechanical Engineers (ASME International) Ocean, Offshore and Arctic Engineering (OOAE) Division, June 2007, OMAE2007-29326.

[36]Jonkman, J.; Butterfield, S.; Musial, W.; and Scott, G., "Definition of a 5-MW Reference Wind Turbine for Offshore System Development," NREL/TP-500-38060, Golden, CO: National Renewable Energy Laboratory, February 2007 (to be published).

[37]Tolman, H. L., "User manual and system documentation of WAVEWATCH-III version 2.22," Environmental Modeling Center Marine Modeling and Analysis Branch (MMAB) Technical Note 222, Washington DC: National Ocean and Atmospheric Administration (NOAA), National Weather Service (NWS), and National Centers for Environmental Prediction (NCEP), September 2002.

[38]van der Tempel, J., "Design of Support Structures for Offshore Wind Turbines," Ph.D. Dissertation, Offshore Engineering Group, Delft University of Technology, Delft, The Netherlands, 2006.

[39]Buhl, M. L., Jr., "Crunch User's Guide," NREL/EL-500-30122, Golden, CO: National Renewable Energy Laboratory, October 2003.

[40]Buhl, M. L., Jr., "CombEEv User's Guide," NREL/EL-500-31664, Golden, CO: National Renewable Energy Laboratory, October 2003.

[41]Greenwood, D. T., *Principles of Dynamics*, 2nd ed., Prentice-Hall, Inc., Englewood Cliffs, NJ, USA, 1998.

[42]Kelley, N. D.; Wright, A. D.; and Osgood, R. M., "A Progress Report on the Characterization and Modeling of a Very Flexible Wind Turbine Design," *A Collection of the 1999 ASME Wind Energy Symposium Technical Papers Presented at the 37th AIAA Aerospace Sciences Meeting and Exhibit, 11–14 January 1999, Reno Nevada, USA*, New York: American Institute of Aeronautics and Astronautics, Inc. (AIAA) and American Society of Mechanical Engineers (ASME), January 1999, pp. 243–252, NREL/CP-500-25513.

REPORT DOCUMENTATION PAGE

Form Approved
OMB No. 0704-0188

PLEASE DO NOT RETURN YOUR FORM TO THE ABOVE ORGANIZATION.

1. REPORT DATE *(DD-MM-YYYY)*	2. REPORT TYPE	3. DATES COVERED *(From - To)*
June 2007	Conference paper	

4. TITLE AND SUBTITLE
Loads Analysis of a Floating Offshore Wind Turbine Using Fully Coupled Simulation: Preprint

5a. CONTRACT NUMBER
DE-AC36-99-GO10337

5b. GRANT NUMBER

5c. PROGRAM ELEMENT NUMBER

6. AUTHOR(S)
J.M. Jonkman and M.L. Buhl Jr.

5d. PROJECT NUMBER
NREL/CP-500-41714

5e. TASK NUMBER
WER7.2902

5f. WORK UNIT NUMBER

7. PERFORMING ORGANIZATION NAME(S) AND ADDRESS(ES)
National Renewable Energy Laboratory
1617 Cole Blvd.
Golden, CO 80401-3393

8. PERFORMING ORGANIZATION REPORT NUMBER
NREL/CP-500-41714

9. SPONSORING/MONITORING AGENCY NAME(S) AND ADDRESS(ES)

10. SPONSOR/MONITOR'S ACRONYM(S)
NREL

11. SPONSORING/MONITORING AGENCY REPORT NUMBER

12. DISTRIBUTION AVAILABILITY STATEMENT
National Technical Information Service
U.S. Department of Commerce
5285 Port Royal Road
Springfield, VA 22161

13. SUPPLEMENTARY NOTES

14. ABSTRACT *(Maximum 200 Words)*

The vast deepwater wind resource represents a potential to use floating offshore wind turbines to power much of the world with renewable energy. Comprehensive simulation tools that account for the coupled excitation and response of the complete system, including the influences of wind-inflow, aerodynamics, structural dynamics, controls, and, for offshore systems, waves, currents, and hydrodynamics, are used to design and analyze wind turbines. The application of such tools in the analysis of floating offshore wind turbines has previously been investigated to only a limited extent. There are numerous possible concepts for floating offshore wind turbine platforms, including a variety of configurations currently used in the offshore oil and gas industries. Coupled analyses are needed to determine their technical and economic feasibility. This paper presents the use of fully coupled aero-hydro-servo-elastic simulation tools to perform a preliminary loads analysis of a 5-MW offshore wind turbine supported by a barge with catenary moorings, which is one of the many promising floating platform concepts.

15. SUBJECT TERMS
Wind; offshore; deepwater; wind costs; loads analysis; loads; hydrodynamics; floating platform; floating; aerodynamics; structural dynamics; structural

16. SECURITY CLASSIFICATION OF:			17. LIMITATION OF ABSTRACT	18. NUMBER OF PAGES	19a. NAME OF RESPONSIBLE PERSON
a. REPORT	b. ABSTRACT	c. THIS PAGE			19b. TELEPHONE NUMBER (*Include area code*)
Unclassified	Unclassified	Unclassified	UL		